

Supergiant Pulses from Extragalactic Neutron Stars

J. M. Cordes ^{*} & Ira Wasserman [†]

Astronomy Department, Cornell University, Ithaca, NY 14853

11 January 2021

ABSTRACT

We consider radio bursts that originate from extragalactic neutron stars (NSs) by addressing three questions about source distances. What are the physical limitations on coherent radiation at GHz frequencies? Do they permit detection at cosmological distances? How many bursts per NS are needed to produce the inferred burst rate $\sim 10^3\text{-}10^4\text{sky}^{-1}\text{day}^{-1}$? The burst rate is comparable to the NS formation rate in a Hubble volume, requiring only one per NS if they are bright enough. However, radiation physics causes us to favor a closer population. More bursts per NS are then required but repeats in 10 to 100 yr could still be negligible. Bursts are modeled as sub-ns, coherent shot pulses superposed incoherently to produce ms-duration ~ 1 Jy amplitudes; each shot-pulse can be much weaker than the burst amplitude, placing less restrictive requirements on the emission process. Nonetheless, single shot pulses are similar to the extreme, unresolved (< 0.4 ns) MJy shot pulse seen from the Crab pulsar, which is consistent with coherent curvature radiation emitted near the light cylinder by an almost neutral clump with net charge $\sim \pm 10^{21}e$ and total energy $\gtrsim 10^{23}$ ergs. Bursts from Gpc distances require incoherent superposition of $\sim 10^{12}d_{\text{Gpc}}^2$ shot pulses or a total energy $\gtrsim 10^{35}d_{\text{Gpc}}^2$ erg. The energy reservoir near the light cylinder limits the detection distance to $\lesssim \text{few} \times 100$ Mpc for a fluence ~ 1 Jy ms unless conditions are more extreme than for the Crab pulsar. Similarly, extreme single pulses from ordinary pulsars and magnetars could be detectable from throughout the Local Group and perhaps farther. Contributions to dispersion measures from galaxy clusters will be significant for some of the bursts. We discuss tests for the signatures of bursts associated with extragalactic NSs.

Key words:

stars:neutron – radio sources – bursts – Crab pulsar – relativistic processes – gravitational lensing: micro.

1 INTRODUCTION

Over the last decade individual radio bursts have been found as a byproduct of surveys for periodic radio pulsars. Reobservations ultimately reveal that many of the sources are radio pulsars, differing only in the means used to initially discover them, but otherwise having similar millisecond pulse widths and dispersion measures (DMs) consistent with a Galactic origin. However, a minority of the bursts has defied redetection. Some are clearly Galactic (e.g. McLaughlin et al. 2006; Spitler et al. 2014, Figure 3) but others have DMs much too large to be accounted for by the modeled foreground interstellar medium (ISM) in the Milky Way. In the literature, bursts found through single-pulse detection algorithms have loosely been referred to as ‘rotating radio transients’ (RRATs; McLaughlin et al. 2006) and are consistent with a Galactic population of neutron stars (NS; Spitler et al. 2014). The more recently discovered events with DMs too large to be accounted for by the Galaxy have been termed ‘fast radio bursts’ (FRBs) (Lorimer et al. 2007; Keane et al. 2011; Thornton et al. 2013; Spitler et al. 2014; Burke-Spolaor & Bannister 2014;

^{*} E-mail: jmc33@cornell.edu

[†] E-mail: ira@astro.cornell.edu

Ravi et al. 2015; Petroff et al. 2015b) and appear to be extragalactic in origin. To avoid confusion, we use the term ‘extragalactic radio burst’ (ERB) for these events.¹

We assume that most if not all of the reported ERBs are in fact astrophysical in nature. Some similar bursts are due to radio-frequency interference (RFI) (‘peryttons;’ Burke-Spolaor et al. 2011; Saint-Hilaire et al. 2014) because they have time-frequency signatures inconsistent with pulsar-like dispersion delays and they have been associated with specific sources of RFI (Petroff et al. 2015c). Though the number of detected ERBs is small, the inferred rate is surprisingly large, $\sim 10^3$ - 10^4 bursts d^{-1} (Keane & Petroff 2015; Law et al. 2015).

In this paper we examine the requirements on radiation coherence and source demographics that are implied by ERB properties summarized in Section 2 and analyze conditions under which they can be met by the population of extragalactic NS. This requires a discussion of coherent radiation bright enough to be detectable in a volume containing enough sources to account for the net observed rate of ERBs for plausible event rates per source. Our paper therefore considers the seemingly disparate topics of radiation physics and populations of compact objects. Other interpretations of ERBs must also consider these issues, so much of our discussion is generic even if NS are not the source population.

The first of these two major topics — radiation — is discussed in Sections 3-5. In Section 3 we summarize giant pulses (GPs) from the Crab pulsar, which serve as exemplars for discussing ERBs. We demonstrate that there is more than enough free energy available to account for observed ERB flux densities emitted from at least 100 Mpc and we consider extension of the pulse-amplitude distribution for the Crab to very long waiting times between super-GPs that might correspond to ERBs. We also emphasize that the largest individual shot pulse ever detected (Hankins & Eilek 2007) is comparable to those required for ERBs and therefore underlies why it is completely reasonable on an empirical basis to consider extragalactic NS as a possible source class for ERBs. Section 4 discusses the shot-noise model that incoherently combines coherent shot pulses in order to match observed ERB properties.

Section 5 considers a specific radiation process, coherent curvature radiation, to demonstrate detailed requirements in the context of a NS magnetosphere. We test our results against the largest Crab shot pulse and find that a large number of leptons ($\sim 10^{29}$) with a relatively small net charge ($\sim 10^{21}$ e) must radiate coherently to account for the measured amplitude; the small net charge reflects the importance of radiation reaction (e.g. Buschauer & Benford 1976). The required charge density in the coherently emitting region is large, perhaps $\sim 10^{11} e \text{ cm}^{-3}$, using coherence volumes (estimated in Appendix B), which are $\gtrsim r_c \lambda^2$ for coherent radiation from charges streaming along field lines with curvature radius r_c . Note that the coherence volume is $\sim (r_c/\lambda) \times \lambda^3 \gg \lambda^3$, i.e. far larger than is often assumed in discussions of coherent radiation (e.g. Kinkhabwala & Thorsett 2000). Nevertheless, the required density is much larger than the Goldreich-Julian density. We do not discuss how these large density contrasts are produced, although we note a few instabilities that might be relevant. Radiation reaction is likely a *generic* issue for understanding ERBs regardless of the class of objects that cause them, including the collapse of supramassive NS (Falcke & Rezzolla 2014), evaporating black holes (Rees 1977), and cosmic strings (Yu et al. 2014), etc.

Section 6 discusses the second major topic — source population requirements — where we estimate event rates per object needed from an extragalactic NS population to yield the large inferred ERB rate. We find that a NS population extending to $z \sim 1$ is large enough that only a few large bursts per NS will suffice to account for the apparent ERB rate. In this case, gravitational microlensing would play a role. However, we favor a closer population for which lensing is unimportant and has less stringent requirements on the radiation process, but requires more bursts per object.

Section 7 summarizes how ERB source populations can be constrained and Section 8 discusses observational tests for features of the NS model for ERBs. Section 9 summarizes our overall results and

¹ For example, an FRB candidate event could be Galactic if the large DM is due to electrons in a Galactic HII region (e.g. Bannister & Madsen 2014), in which case the source might be termed an RRAT.

conclusions. Appendix A gives the calculation of flux densities of single and incoherently-combined shot pulses. Appendix B presents the calculation of coherence volumes in dipolar magnetospheres.

2 SALIENT FEATURES OF ERBS

ERBs have fundamental properties that need to be accounted for in any interpretation. First, millisecond duration pulses with flux densities ~ 1 Jy must originate from compact sources with relativistic flows. The radiation must have high spatial coherence to produce the very high inferred brightness temperatures,

$$T_b = \frac{S_\nu}{2k} \left(\frac{d}{\nu \Delta t} \right)^2 \sim 3 \times 10^{35} \text{K} S_{\nu, \text{Jy}} (d_{\text{Gpc}} / \nu_{\text{GHz}} \Delta t_{\text{ms}})^2, \quad (1)$$

where distances are in Gpc and the burst duration has been associated with the light-travel time across the source. ERBs therefore are not unlike pulses from Galactic pulsars and RRATs so they could have similar underlying radiation physics.

Second is that ERBs, like pulsar pulses, have radiation time scales that must span a range from $\lesssim 1$ ns to $\gtrsim 1$ ms. Nanosecond structure necessarily follows from the GHz frequencies at which ERBs have been detected while ERBs manifestly show total widths up to a few milliseconds. Shot noise models with variable amplitudes or rates naturally account for these features.

Third, while arguments have been made that the high dispersion measures of ERBs originate from or are mimicked by an emission process in the sources themselves (e.g. Kulkarni et al. 2014; Loeb et al. 2014), the simplest interpretation at present is that the burst sources are extragalactic (e.g. Luan & Goldreich 2014; Dennison 2014). Connor et al. (2015) suggest that the non-Galactic portions of ERB DMs are dominated by plasma in supernova shells from relatively nearby (non-cosmological) galaxies. Extragalactic distances require larger radio luminosities than typical radio pulsars, however, and one goal of this paper is to examine whether coherent processes in neutron-star (NS) magnetospheres (or similar objects) can produce detectable bursts originating from large distances.

Finally, despite the small number found so far, the implied aggregate event rate $\sim 10^3$ - 10^4 day $^{-1}$ over the entire sky is astonishingly large (Law et al. 2015; Keane & Petroff 2015), much larger than the observed rate of gamma-ray bursts, for example (Thornton et al. 2013; Spitler et al. 2014). The lack of any new events in reobservations of ERB sky directions requires either that ERBs originate from non-repeating astrophysical cataclysms or from repetitive sources with very low burst rates. Until a distance scale is established for ERBs, it is not possible to identify any particular underlying source class. However, in this paper we find that extragalactic NS could account for the burst properties observed so far.

3 MAXIMAL RADIO EMISSION FROM PULSARS

In this section we summarize large-amplitude coherent radiation from pulsars as a benchmark for discussion of ERB radiation. Rotation-driven NS dissipate their energy through emission in particles accelerated by rotationally-generated electric fields, low-frequency waves, and high-energy radiation. It is well known from early studies of pulsars that relativistic particles have significant energy losses from coherent radio emission (Sturrock 1970, 1971; Ruderman & Sutherland 1975; Buschauer & Benford 1976). It follows, therefore, that the amplitudes and durations of narrow pulses are limited by radiation reaction, a point emphasized by Buschauer & Benford (1980) in their analysis of the Crab pulsar. But this also means that coherent radio emission can tap a sizable fraction of the free energy available in particles. Radio emission is typically a tiny fraction of the spindown energy loss rate, $\dot{E} = I\Omega\dot{\Omega}$ (Ω = spin frequency and I = moment of inertia), particularly for the average emission from objects with large values of \dot{E} , such as the Crab pulsar. However, some older, long-period pulsars have $L_r/\dot{E} \sim 1$ - 10% (e.g. Arzoumanian et al.

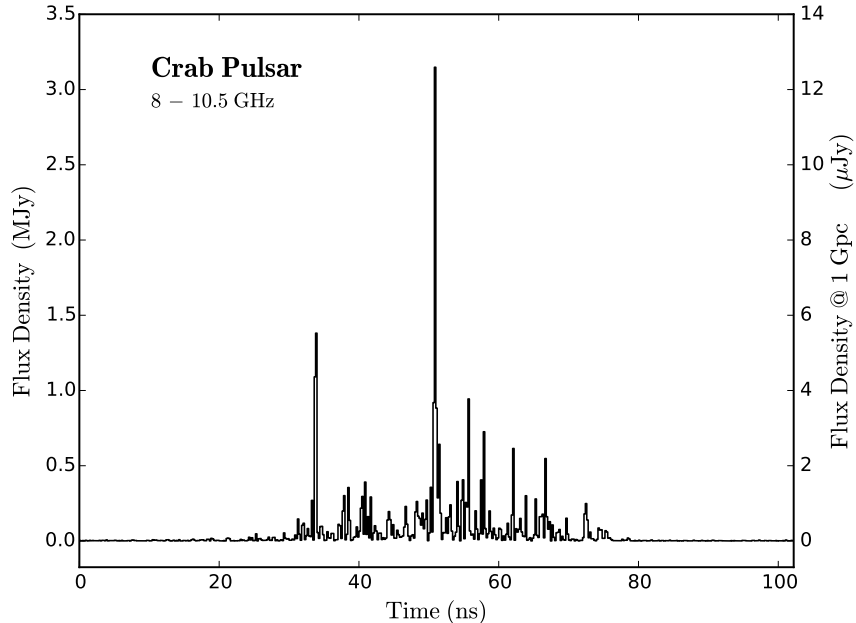


Figure 1. Portion of a single pulse from the Crab pulsar showing sub-ns structure (data courtesy of Hankins & Eilek (2007)) that is consistent with a shot-pulse model for the radiation. The largest shot pulse exceeds 3 MJy and several others exceed 0.5 MJy. The right-hand axis indicates the flux-density scale if the source were at a 1 Gpc distance;

2002). Recent work has also revealed a direct link between radio emission and \dot{E} in intermittent pulsars showing on-and-off intensity transitions that accompany large changes in \dot{E} (e.g. Kramer et al. 2006).

3.1 Giant Pulses from the Crab Pulsar

In this paper, we use GPs from the Crab pulsar as benchmarks in several ways. First, we can extrapolate the amplitudes of GPs to those of young-pulsar analogs in other galaxies and consider whether they can serve as an underlying population for ERBs. Second, ERBs may originate from older NS due to triggering by unknown agents of Crab GP type emission. Third, the narrowest features seen on ns time scales in a few Crab GPs provide evidence for extremely bright emission from individual coherently radiating regions that can be superposed in large numbers to provide detectable pulses from large distances. Thus, ERBs might be from young pulsars but they need not be.

The brightest GP detected so far had a peak amplitude $S_{\nu, \max} = 2.2$ MJy at 9 GHz and a pulse width Δt smaller than the 0.4 ns time resolution provided by the 2.5 GHz receiver bandwidth (Hankins & Eilek 2007). The implied brightness temperature $T_b \gtrsim 10^{41.3}$ K obviously requires a coherent emission process. The upper bound on Δt implies a time-bandwidth product $\nu \Delta t \lesssim 4$, suggesting that it is a single shot pulse produced by an individual, coherently emitting region. Figure 1 shows this pulse with higher analysis resolution and a slightly different flux-density (T. Hankins and J. Eilek, private communication). Unlike this special case, most GPs, like all pulsar radiation, have time-bandwidth products $\nu \Delta t \gg 1$ because they are *incoherent superpositions of shot pulses*. Relatively frequent GPs at 0.43 GHz with ~ 100 -200 kJy maxima occur about once per hour (Hankins & Rickett 1975; Cordes et al. 2004; Crossley et al. 2010). They are broadened by interstellar scattering to $\sim 100 \mu s$ from intrinsic widths of about $50 \mu s$. The implied time-bandwidth product $\sim 50 \mu s \times 0.43 \text{ GHz} \sim 2 \times 10^4$ requires a combination of coherent emission and incoherent superposition and this is consistent with the appearance of single GPs obtained with high time resolution. The same can be said of pulsar signals generally.

Giant pulses from the Crab pulsar comprise $\sim 1\%$ of all pulses and have an amplitude distribution that shows no discernible cutoff in data sets as large as 100 hr of on-pulsar live time ($\sim 10^7$ pulse periods) (Lundgren et al. 1995; Mickaliger et al. 2012). Fits of power-law distributions $\propto S_\nu^{-\alpha}$ yield exponents ranging from $\alpha \approx 2.3 - 3.5$ in observations at different frequencies (Mickaliger et al. 2013). The power-law component may be augmented with a long tail associated with additional, supergiant pulses (SGPs) (Cordes et al. 2004; Mickaliger et al. 2012), but with as-yet poorly constrained parameters for the tail. The existence of SGPs from the Crab pulsar suggests that much larger pulses from it and other objects may be seen only in monitoring campaigns that are much longer than those conducted to date.

3.2 GP Energetics

The largest GPs from the Crab pulsar are easy to accommodate within the total energy-loss budget of its magnetosphere but require significant fractions of the available particle energies to be directed into coherent emission.

We relate maximal GP emission to the spindown energy loss rate $\dot{E} \sim 10^{38.7}$ erg s $^{-1}$ by combining the radio emission efficiency $\epsilon_r \leq 1$ with the beaming solid angle Ω_r into a combined factor $\zeta_r = (4\pi\epsilon_r/\Omega_r)$. The peak flux density is then

$$S_{\nu,\max} = \left(\frac{4\pi\epsilon_r}{\Omega_r} \right) \left(\frac{\dot{E}}{4\pi\Delta\nu_r d_{\text{Crab}}^2} \right) \approx \frac{100\zeta_r \text{ MJy}}{\Delta\nu_{\text{GHz}}} \left(\frac{\dot{E}_{38}}{4.6} \right). \quad (2)$$

The approximate equality uses parameter values for the Crab pulsar including $d_{\text{Crab}} = 2$ kpc. Evaluating for the 2 MJy shot pulse at 9 GHz and the more frequent ~ 100 kJy pulses at 0.43 GHz, we obtain $\zeta_r = 0.02$ and 0.002, respectively. We may expect infrequent but very large pulses from the Crab pulsar when $\zeta_r \gg 1$, which may occur as a consequence of favorable relativistic beaming or large instantaneous departures from the average radio efficiency ϵ_r .

The ‘Crab twin’ pulsar B0540–69 in the Large Magellanic Cloud ($P = 50$ ms, $B = 5 \times 10^{12}$ G) also shows giant pulses (Johnston & Romani 2003) but with $S_{\nu,\max} d_{\text{B0540-69}}^2$ smaller by a factor ~ 0.1 than those of the Crab pulsar. Some of the difference could be due to less-favorable beaming for B0540–69.

While GPs can be accommodated by spindown losses, they may saturate the typical energy available in relativistic particles. Force-free conditions $\mathbf{E} \cdot \mathbf{B} = 0$ in a neutron-star’s magnetosphere require a charge (number) density $n_{\text{GJ}} \approx -\Omega \cdot \mathbf{B}/2\pi ec$, the Goldreich-Julian (GJ) density,

$$n_{\text{GJ}0} \approx 10^{10.84} \text{ cm}^{-3} B_{12} P^{-1} (R/r)^3, \quad (3)$$

where the radial scaling applies to the open-field-line region of a dipolar magnetosphere with $r \geq R$, where R is the NS radius, and $r \ll r_{\text{lc}}$ where the light-cylinder radius is $r_{\text{lc}} = cP/2\pi$. For standard $\sim 10^{12}$ volt potential drops in polar cap models (e.g. Ruderman & Sutherland 1975; Michel 1982, Table V), the particle energy loss rate (assuming an electron mass) is approximately

$$\dot{E}_p = cA_{\text{pc}} n_{\text{GJ}} \gamma m c^2 \approx 10^{30} \text{ erg s}^{-1} B_{12} R_6^3 \gamma_6 P^{-2} \propto \dot{E}^{1/2}, \quad (4)$$

for a Lorentz factor γ and a magnetic polar cap area $A_{\text{pc}} \approx \pi R^3/r_{\text{lc}} \propto P^{-1}$. The particle loss rate scales as the square root of the spindown loss rate in standard polar-cap models (Ruderman & Sutherland 1975; Arons & Scharlemann 1979). The Crab pulsar ($B_{12} = 3.78$ and $P^{-1} = 30.2$ Hz) yields $\dot{E}_p \simeq 10^{33.7}$ erg s $^{-1}$. For the 9-GHz pulse described above, highly beamed radiation with $\Omega_r/4\pi \lesssim 2 \times 10^{-4}$ is required to provide $L_r \lesssim \dot{E}_p$. Since the beam solid angle is likely even smaller than this limit for $\gamma \gtrsim 10^3$, there is significant headroom in the possible range of GP amplitudes to the extent that particle flows and radiation physics can allow much larger values.

3.3 Extrapolation of Rates and Amplitudes from the Crab Pulsar

The maximum detectable distance of a Crab GP with amplitude $S_\nu = 10^5$ Jy is $d_{\max} = d_{\text{Crab}} (S_\nu/S_{\nu,\min})^{1/2} \approx 2.5$ Mpc – a distance that encompasses most local-group galaxies – for a detection threshold $S_{\nu,\min} = 60$ mJy (e.g. a 5σ detection for an Arecibo-class telescope²). Flux densities about 10^5 times brighter ($\sim 10^{10}$ Jy) are needed for analogous objects to be detectable 1 Gpc away.

We scale from Crab GPs to fiducial Gpc distances using

$$S_{\nu,\max} = S_{\nu,\max,\text{Crab}} \left(\frac{\zeta_r}{\zeta_{r,\text{Crab}}} \right) \left(\frac{d_{\text{Crab}}}{d} \right)^2 \left(\frac{\dot{E}_{38}}{4.6} \right) \approx 0.2 \mu\text{Jy} \frac{\dot{E}_{38}}{\Delta\nu_{\text{GHz}} d_{\text{Gpc}}^2} \left(\frac{\zeta_r}{\zeta_{r,\text{Crab}}} \right). \quad (5)$$

Pulses with $S_\nu \sim 1$ Jy require a combination of larger ζ_r (i.e. larger radio efficiency or smaller beaming solid angle) with larger spindown loss rates \dot{E} and distances smaller than 1 Gpc. To be detectable at 1 Gpc with a 60 mJy threshold, $(\zeta_r/\zeta_{r,\text{Crab}})\dot{E}_{38} \gtrsim 3 \times 10^5$. Objects undoubtedly exist with spindown loss rates $\dot{E} \propto \dot{P}P^{-3}$ much larger than that of the Crab pulsar. This could include the Crab pulsar itself when it was born with $P \sim 20$ ms compared to its present-day 33 ms period (e.g. Michel 1991). Magnetars with 100 times larger magnetic fields could have \dot{E} up to 10^6 times larger than the Crab pulsar’s loss rate if they are born with 10 ms periods. However, their birthrate is small and they spend little time at short periods if measured spin down time scales at longer periods can be extrapolated to earlier times (c.f. Olausen & Kaspi 2014, Table 2). Magnetars are therefore less likely to be responsible for ERBs unless they are relatively nearby.

3.4 Extreme-Value Statistics and Waiting Times

We now consider the sampling of pulses from a single object in terms of the probability density function (PDF) $f_1(S)$ and the cumulative distribution function (CDF) $F_1(S)$ for their amplitudes, where the subscript ν on S is dropped to simplify the notation. Most pulsars do not show GPs and have PDFs that are typically consistent with log-normal distributions (Burke-Spolaor et al. 2012). GP amplitude PDFs, however, are heavy tailed with a power-law type shape for a sizable range of pulse amplitudes. By ‘heavy tailed’, we mean that the PDF extends to amplitudes much larger than the mean.

We adopt a power law³ PDF, $f_1(S) \propto S^{-\alpha}$ between lower and upper cutoffs S_l and S_u . For steep power laws, an increasingly larger maximum S is expected as the number of sampled pulses increases. Consider N pulses occurring periodically in time $T = NP$ with period P and amplitudes drawn from $f_1(S)$. The maximum amplitude has a CDF equal to the probability that all amplitudes are less than or equal to S . The extreme value CDF and PDF are therefore

$$F_N(S) = [F_1(S)]^N \quad \text{and} \quad f_N(S) = N f_1(S) [F_1(S)]^{N-1}. \quad (6)$$

Figure 2 (left) shows a sequence of extreme-value PDFs for $\alpha = 3$ and $S_u/S_l = 10^8$, which maximize at steadily larger flux densities as N increases from 1 to 10^{12} . Each PDF is marked by its mode. For $\alpha \neq 1$, $S_{\text{mode}} = S_l [1 - (N-1)(1-\alpha)/\alpha]^{1/(\alpha-1)}$. The median is given by $S_{\text{med}} = [1 + e^{-(\ln 2)/N} (S_l/S_u)^{\alpha-1}]^{-1/(\alpha-1)}$.

A similar approach can be applied to pulses emitted with Poisson statistics. The CDF is obtained by summing $F_N(S)$ over the Poisson probabilities for obtaining N pulses given a mean number $\langle N \rangle$ in time T . This approach would also be valid for the Crab pulsar because pulses with amplitudes above a fixed threshold occur at intervals consistent with Poisson statistics (Lundgren et al. 1995). The two approaches yield very similar results and in the following, we use expressions for the periodic case.

² Assuming a bandwidth of 50 MHz and a system equivalent flux density of 4 Jy along with a matched filter with 1 ms width.

³ A pure power-law model does not always appear to be a good model for histograms of pulse amplitudes from the Crab pulsar. However, they always show long tails so we proceed by using power-law PDFs to make extrapolations while keeping in mind that the true form of the PDF may differ.

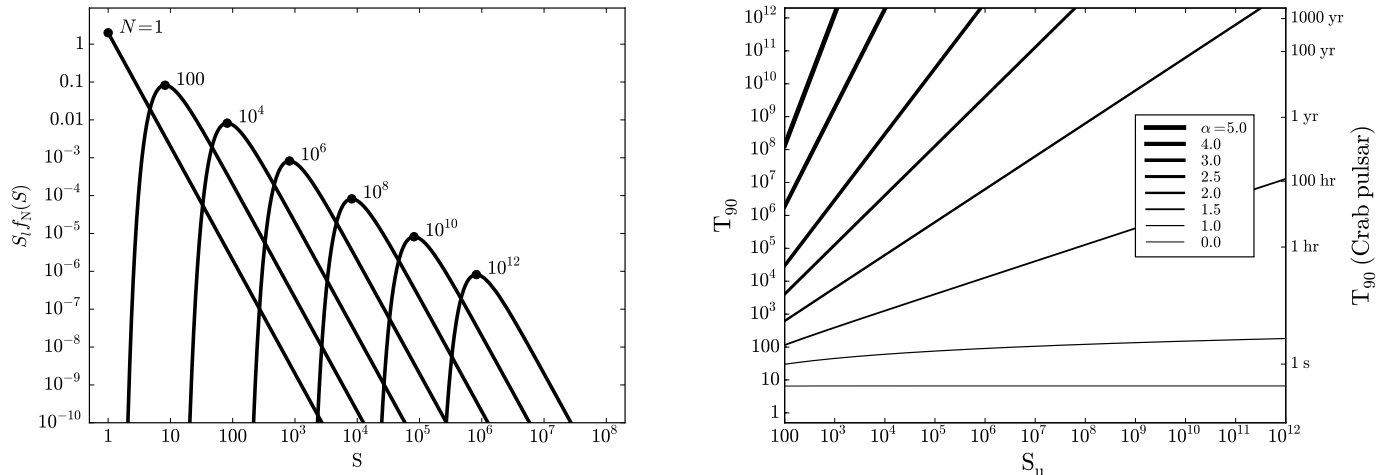


Figure 2. Left: PDF of maximum $S = rS_l$ for $\alpha = 3$ and $r_u = S_l/S_u = 10^8$ for various N . The filled circles denote the modes of the PDFs. Right: Time T_{90} (expressed in units of pulse period) to reach 90% of the maximum amplitude r_u for different values of α . The right-hand scale gives T_{90} in time units using the spin period $P = 0.033$ s of the Crab pulsar.

The time needed to see the largest pulses spanned by the PDF $f_1(S)$ is strongly dependent on the upper cutoff S_u and on α . For any specified S , the waiting time needed to see an amplitude as large as the median of $f_N(S)$ is obtained by solving $F_N(S) = 1/2$,

$$T = -P \ln 2 / \ln F_1(S). \quad (7)$$

If we specify a median that is within a factor $f_u < 1$ of the largest possible amplitude S_u , the waiting time is

$$T_f = -P \ln 2 / \ln F_1(f_u S_u). \quad (8)$$

Figure 2 (right) shows T_f for $f_u = 0.9$ and multiple values of α that demonstrate the reasonable result that steeper distributions (larger α) with larger upper cutoffs S_u require longer times to reach 90% of the cutoff. Flatter distributions, however, can be sampled in small amounts of time. The waiting times are 10^{12} periods ($\sim 10^3$ yr) or larger for $\alpha \gtrsim 2$ and $S_u/S_l = 10^{12}$. Since previous studies, as noted earlier, indicate $\alpha \sim 2.3$ to 3.5 for Crab-pulsar GPs, the possibility remains that much larger pulses will occur if S_u is large and observations extend over time spans much longer than the 100 hr of previous studies. Conversely, continued monitoring of GPs from the Crab pulsar can determine or place a lower bound on the upper cutoff S_u . Knowledge of the cutoff can help establish the distance scale of any extragalactic GP-emitting objects, including ERBs under the GP hypothesis, or it could rule out the hypothesis if S_u is not substantially larger than GPs seen to date from the Crab pulsar. The Bayesian posterior PDF for S_u can be evaluated from an observation of the largest pulse $S_{\max}(T)$ seen in a time span T using assumed values for S_l and α based on previous measurements. For steep power laws, the resulting lower bound will be a modest multiple of $S_{\max}(T)$. We remark here that in Section 5.3 our analysis of radiation physics suggests that the largest possible giant pulses from the Crab pulsar may be constrained by the maximum fluence of individual coherent emitting structures. If so, larger amplitude GPs would require greater numbers of coherent structures summing incoherently.

Now we compare the median amplitudes $S_{1,2}$ expected in two time intervals, $T_1 < T_2$. From Eq. 7,

$$\frac{T_2}{T_1} = \frac{\ln F_1(S_1)}{\ln F_1(S_2)} \approx \frac{1 - F_1(S_1)}{1 - F_2(S_2)}. \quad (9)$$

Solving for S_2 , we obtain

$$S_2 \approx S_1 \left(\frac{T_2}{T_1} \right)^{1/(\alpha-1)} \left[1 + (S_1/S_u)^{\alpha-1} (T_2/T_1 - 1) \right]^{-1/(\alpha-1)} \approx S_1 \left(\frac{T_2}{T_1} \right)^{1/(\alpha-1)}, \quad (10)$$

where the approximate equality holds for $(T_2/T_1)(r_1/r_u)^{\alpha-1} \ll 1$. Using the $S_1 \sim 100$ kJy pulse typically seen from the Crab pulsar in $T_1 =$ one hour (c.f. Section 3.1), and using power-law indices that have been inferred ($\alpha \approx 2.3 - 3.5$) to extrapolate to long times, the largest pulse expected in 10^3 yr using Equation 10) is $S_2 = 10^{7.7}$ Jy ($\alpha = 3.5$) to $10^{10.3}$ Jy ($\alpha = 2.3$). The corresponding maximum detection distances are $d_{\max} = 15$ Mpc to 300 Mpc using $d_{\max} = 0.63$ Mpc $(T/1 \text{ hr})^{1/2(\alpha-1)}$.

3.5 Implications for Weak and Strong ERBs

We have shown in the previous section that a power-law PDF for GPs can lead to very long waiting times for the largest pulses if a steep PDF extends to very high values. Here we consider the expected number of weaker pulses above some threshold in the same time interval containing a very bright pulse. The number of detected pulses, defined as those exceeding a threshold S , out of N total pulses is, on average, $N_d(S) = N [1 - F_1(S)]$. From this N can be expressed in terms of S_{\max} and N_d . The brightest pulse S_{\max} corresponds to $N_d(S_{\max}) = 1$, so the number above a lower threshold $S_{\text{th}} < S_{\max}$ is

$$N_d(> S_{\text{th}}|S_{\max}) = N [1 - F_1(S)] = \left(\frac{S_{\max}}{S_{\text{th}}} \right)^{\alpha-1} \left[\frac{1 - (S_{\text{th}}/S_u)^{\alpha-1}}{1 - (S_{\max}/S_u)^{\alpha-1}} \right] \approx \left(\frac{S_{\max}}{S_{\text{th}}} \right)^{\alpha-1}, \quad (11)$$

where the approximate expression is for $S_{\text{th}}, S_{\max} \ll S_u$. For a threshold a factor of ten lower than the maximum pulse, we expect $N_d(> S_{\text{th}}|S_{\max}) \approx 10^{\alpha-1}$ or 20 to 320 weaker pulses for $\alpha = 2.3$ to $\alpha = 3.5$, respectively.

Extrapolation from the Crab pulsar to an individual ERB source suggests that a large number of weak pulses should be seen for the cases where the ERB detection is well above an overall detection threshold. The four ERBs detected by Thornton et al. (2013) are above threshold by factors of 1.2 to 5.4. However, the dwell time on each sky position was only 270 s, so the expectation of a larger number of weaker pulses depends heavily on assumptions about the overall *population* of ERB sources. The Lorimer burst (Lorimer et al. 2007) exacerbates the situation because its amplitude is 100 times threshold, but the overall issues about the luminosity function and spatial distribution of ERB sources remain the same.

If all sources have the same intrinsic amplitude PDF, weaker pulses should have been detected from all of the ERB sources at the same distance as, for example, that of the largest of the four ERBs. Additionally, a uniform population of sources would produce a population PDF $\propto S^{-5/2}$ in Euclidean space for standard-candle luminosities or a broader distribution for the intrinsic power-law PDF considered above.

That weaker pulses have not been detected suggests several alternatives. One is that the amplitude distribution for ERBs is dissimilar from the steep power law seen for most of the GPs from the Crab pulsar. The Crab pulsar itself suggests that supergiant pulses (SGPs) occur as a long tail with a different distribution than ‘regular’ GPs (Cordes et al. 2004; Mickaliger et al. 2012), as mentioned in Section 3.1. To account for the absence of weaker ERBs in Thornton et al.’s results, a suitable intrinsic amplitude PDF would have to be combined with a spatial population distribution that excludes the continuous, steep *net* amplitude PDF expected in Euclidean space for standard candles (or for any given luminosity out of a broad luminosity function). One possibility is for the spatial distribution to be highly clustered so that there is a gap in the population amplitude PDF not far above the amplitudes of the ERBs detected so far.

Stronger pulses (than ERBs observed so far) are not an issue (yet) in spite of the large number of ERB sources needed to account for the inferred all-sky rate. Suppose the four ERBs detected by Thornton et al. (2013) originate from the same distance D_{FRB} and from a standard candle distribution, while ignoring the differences in amplitude (which are not large but are influenced by pulse-scattering broadening for

one out of the four and by off-axis telescope gain differences). Any nearer sources are fewer in number for a uniform source density, so less than one, stronger ERB is expected for distances $D < 4^{-1/3} D_{\text{FRB}}$ corresponding to amplitudes $S > 2.5 S_{\text{ERB}}$. A corresponding statement can be made for a non standard-candle distribution. Radiation physics may provide a maximum possible luminosity that would cap the maximum observable amplitude.

We consider these issues further in the next three sections that consider ERB radiation physics and population distributions.

4 SHOT NOISE MODEL FOR ERBS

The fundamental unit of radio emission is a coherent shot pulse with unit time-frequency product (a consequence of Fourier transforms), so detection at radio frequencies $\nu \gtrsim 1$ GHz requires widths $W_s \lesssim 1$ ns. Actual pulses have large time-frequency products $\nu W_i \gg 1$ because they are incoherent combinations of coherent shot pulses. In this section we discuss the requirements for generating shot pulses that are sufficiently bright and numerous to account for ERB amplitudes after they are combined incoherently.

4.1 Maximal Shot Pulse Amplitudes

First we calculate the maximum possible radiation from a single coherently-emitting entity so that we can quantify the number of shot pulses needed to account for the amplitudes of ERBs and then assess plausible maximum distances of ERB sources. ERB detections may in fact involve observational selection of extreme physical conditions. An individual emitter might be a charge clump in the relativistic flow of a magnetosphere (Weatherall & Benford 1991; Weatherall 1998; Hankins et al. 2003; Asseo & Porzio 2006). Clumps may be produced from a two-stream instability or a bunching instability associated with coherent synchrotron radiation (Goldreich & Keeley 1971; Buschauer & Benford 1978; Schmekel et al. 2005; Schmekel & Lovelace 2006; Schmekel 2005).

A simple estimate for maximum possible shot-pulse amplitudes is as follows. Consider a dense, relativistic charge clump that radiates a fraction ϵ_E of its total energy $E_N = N\gamma mc^2$ (N = number of particles) into a solid angle $\Delta\Omega \sim \gamma^{-2}$ in a time W_s as seen by an observer. The unit time-bandwidth product of the pulse implies that the spectrum extends to an upper frequency $\nu_s \sim 1/W_s$ with a spectral shape $f(\nu)$ normalized to unit area. For a receiver bandwidth $\Delta\nu_r \ll \nu$ at a centre frequency $\nu \lesssim \nu_s$ and a source distance $d = 1 \text{ Gpc } d_{\text{Gpc}}$, the peak flux density of the shot pulse⁴ is (c.f. Appendix A)

$$s_{\nu, \text{max}} = \frac{\epsilon_E E_N \Delta\nu_r f(\nu)}{\Delta\Omega d^2} = \frac{\epsilon_E \gamma^3 N m c^2 \Delta\nu_r f(\nu)}{(\gamma^2 \Omega) d^2} \approx 10^{-29} \epsilon_E N \gamma_3^3 d_{\text{Gpc}}^{-2} (\gamma^2 \Omega)^{-1} \Delta\nu_r \text{GHz} f(\nu) \text{ Jy}, \quad (12)$$

where the electron mass has been used to evaluate the expression and the factor $\gamma^2 \Omega$ indicates that the relevant solid angle may differ from the assumed $\Omega = \gamma^{-2}$. A 1-Jy shot pulse at $d = 1 \text{ Gpc}$ requires the energy in *at least* $N = 10^{29} \epsilon_E^{-1}$ electrons and/or positrons for nominal values of other parameters in this estimate.

The required number of particles can be expressed as $N = \eta_{\text{GJ}} \eta_V n_{\text{GJ0}} \lambda^3$ where η_{GJ} is a multiplier of the surface GJ density n_{GJ0} (Equation 3) and $\mathcal{V}_c = \eta_V \lambda^3$ is the ‘coherence’ volume from which particles produce a coherent pulse measured by an observer. It is often assumed that $\mathcal{V}_c \sim \lambda^3$ or $\eta_V \sim 1$ (e.g. Benford & Buschauer 1977; Sallmen et al. 1999; Kinkhabwala & Thorsett 2000), but for relativistic motion in a magnetic dipole, we find $\eta_V \gg 1$ (Appendix B). To provide the number of particles, the combined

⁴ Here and in Appendix A we use lower-case s_ν to designate the flux density of a shot pulse and upper case S_ν for the macroscopic ERB pulse comprising an ensemble of shot pulses.

multiplier must satisfy

$$\eta_{\text{GJ}}\eta_{\text{V}} \approx 10^{14} \frac{P\nu_{\text{GHz}}^3}{\epsilon_E \gamma_3^3 \Delta\nu_r f(\nu) B_{12}} \left(\frac{s_{\nu, \text{max}} d^2}{1 \text{ Jy Gpc}^2} \right), \quad (13)$$

where we have substituted for the surface GJ density from Eq. 3. The required multiplicity factor can be reduced significantly under several conditions: shot pulses that have peak flux densities $s_{\nu, \text{max}} \ll 1 \text{ Jy}$; small spin periods, large magnetic fields and Lorentz factors, and distances less than 1 Gpc.

As calibration of our analysis, we revisit the 2 MJy shot pulse from the Crab pulsar at 9 GHz, which becomes 2 μJy if emitted at 1 Gpc, or $s_{\nu, \text{max}} d^2 = 8 \text{ MJy kpc}^2 = 8 \times 10^{-6} \text{ Jy Gpc}^2$. This shot pulse itself requires a large multiplier,

$$(\eta_{\text{GJ}}\eta_{\text{V}})_{\text{Crab}} \approx \frac{10^{9.7} d_{\text{Gpc}}^2}{\epsilon_E \gamma_3^3 \Delta\nu_r}. \quad (14)$$

Pair production accounts for some of the multiplicity, typically 10^3 to 10^4 in pulsar models (e.g. Ruderman & Sutherland 1975), and an e^\pm Lorentz factor $> 10^3$ could decrease the required value. The remaining multiplicity can come from the volume factor. Emission far from the NS surface increases the required multiplicity because the particle density scales as r^{-3} , so high altitude emission regions require a volume multiplier comparable to that needed for ERBs.

4.2 Incoherent Summation of Shot Pulses

An empirical description of pulses from both pulsars and ERBs is the amplitude modulated noise model (AMN; Rickett 1975) in which a Gaussian noise process with characteristic time scales $\lesssim \nu^{-1} \lesssim 1 \text{ ns}$ is modulated on time scales of microseconds and longer. While the AMN model is an adequate statistical description of macroscopic pulses, a better physical description is amplitude and rate modulated shot noise, a sequence of shot pulses with a time-dependent Poisson rate (Cordes 1976; Cordes et al. 2004; Ostrowski et al. 2011; Gwinn et al. 2011). In Appendix A we demonstrate that amplitude and rate modulations are indistinguishable unless individual shot pulses can be identified in high-resolution time series. ERBs are too weak to allow detection of individual shot pulses and the extragalactic hypothesis implies that sources at Gpc distances will require the rate of shot pulses to be large, much larger than shown in Figure 1.

Eq. A9 gives the peak flux density $S_{\nu, \text{max}}$ for an ERB lasting W_i (e.g. $\sim 1 \text{ ms}$) in terms of the number of incoherently-combined shot pulses N_i of amplitude $s_{\nu, \text{max}}$. For time resolution $W_r = \Delta\nu_r^{-1}$ with a receiver bandwidth $\Delta\nu_r$,

$$S_{\nu, \text{max}} \approx (W_r/W_i) N_i s_{\nu, \text{max}}. \quad (15)$$

The peak flux density is smaller than the flux density summed over all shot pulses $\sim N_i s_{\nu, \text{max}}$ by the factor $W_r/W_i \ll 1$. Smoothing of the intensity does not change this result (Appendix A) because the frequency range of the receiver is the determining factor. For example, $W_i = 1 \text{ ms}$ and $W_r = 10 \text{ ns}$ for a receiver with a 100 MHz bandwidth, yielding $W_r/W_i \sim 10^{-5}$. If N_i is very large, individual shot pulse amplitudes $s_{\nu, \text{max}}$ can be much smaller than the measured peak flux density $S_{\nu, \text{max}}$.

To investigate what is required, let the ERB arise from a volume $\mathcal{V}_i \sim (cW_i)^3$ containing N_i coherently-emitting regions that produce incoherently combined shot pulses. Each has a subvolume \mathcal{V}_c so the ensemble of N_i regions fills a volume $N_i \mathcal{V}_c \equiv \zeta_{\text{ff}} \mathcal{V}_i$, where $\zeta_{\text{ff}} < 1$ is a volume filling factor, or $N_i = \zeta_{\text{ff}} \mathcal{V}_i / \mathcal{V}_c$. Eq. (B7) indicates that the characteristic size of the coherent volume is $\mathcal{V}_c / (cW_s)^3 \lesssim \omega r_c / c \sim \gamma^3$ if the coherent radiation at frequency $\nu = \omega / 2\pi$ is from particles streaming along magnetic field lines with radius of curvature r_c ; actual values are model dependent and may be larger or smaller than this value. The

typical peak shot-pulse amplitude is then

$$s_{\nu,\max} \approx \frac{S_{\nu,\max}}{N_i} \frac{W_i}{W_r} = \frac{S_{\nu,\max}}{\zeta_{\text{ff}}} \frac{\mathcal{V}_c}{\mathcal{V}_i} \frac{W_i}{W_r} \lesssim \frac{S_{\nu,\max}}{\zeta_{\text{ff}}} \frac{\gamma^3 W_s^3}{W_i^3} \frac{W_i}{W_r} = \frac{S_{\nu,\max}}{\zeta_{\text{ff}}} \frac{(\gamma W_s)^3}{W_i^2 W_r} \sim 0.1 S_{\nu,\max} \frac{\Delta\nu_{r,\text{GHz}} (\gamma_3 W_{s,\text{ns}})^3}{\zeta_{\text{ff}} W_{i,\text{ms}}^2}. \quad (16)$$

For nominal values in the rightmost equality, shot pulses are 10% of the ERB amplitude. However this is an upper bound and the shot pulse width may be substantially shorter than 1 ns. Observed widths are somewhat larger than 1 ms, although scattering in the ISM or intergalactic medium (IGM) may account for some of the observed widths. Shot pulses therefore could be much smaller than the ERB amplitude by six orders of magnitude or more if the filling factor is not small. This means that 1 Jy ERBs could be accounted for by shot pulses that are similar in pseudo-luminosity to the MJy shot pulse from the Crab pulsar.

5 COHERENT CURVATURE RADIATION

Using general arguments we have shown in Section 4 that the largest shot pulse seen from the Crab pulsar requires extreme radiation efficiency and particle concentration; even more extreme conditions are required to produce \sim Jy shot pulses from distances \sim Gpc. However, incoherent summation of shot pulses, as noted, can allow the required shot pulse amplitudes to be comparable to the maximum seen so far from the Crab pulsar. Here we derive the requirements for the specific case of curvature radiation.

5.1 Fractional Clump Charge

A simple estimate of the net fractional charge that can produce a consistent result is as follows. A single electron moving on a curved path with radius $r_c = 10^9 r_{c,9}$ cm radiates power $P_1 = 2\gamma^4 e^2 c / 3r_c^2$ (e.g. Jackson 1962) and has a long radiation lifetime,

$$\tau_1 = \frac{\gamma m_e c^2}{P_1} = \frac{3}{2} \frac{r_c^2}{\gamma^3 r_e c} = 10^{11.2} s \gamma_3^{-3} r_{c,9}^2. \quad (17)$$

The lifetime of N charges of the same sign radiating coherently at a rate $P_N = N^2 P_1$ is $\tau_N = \tau_1 / N$. A shot pulse with observed duration $r_c / \gamma^3 c$ corresponds to a time interval $r_c / \gamma c$ over which the clump radiates toward the observer. However, if radiation losses cause the clump lifetime to be shorter than this time, $\tau_N < r_c / \gamma c$, the observed pulse width will be narrower, τ_N / γ^2 , and the spectrum correspondingly wider.

For the nominal particle number $N \sim 10^{29} \epsilon_E^{-1}$ calculated earlier, the lifetime $\tau_N = 10^{-17.8} \epsilon_E^2 s$ is far too short to yield enough power in the radio band. The solution is for the clump of N particles to be nearly charge neutral. Letting the effective charge be $Q_e e$, the clump lifetime becomes $\tau_c = N \tau_1 / Q_e^2$ and matching it to $r_c / \epsilon_E \gamma c$ yields

$$\frac{Q_e}{N} = \left(\frac{\epsilon_E \gamma c \tau_1}{N r_c} \right)^{1/2} = \left(\frac{3 r_c \epsilon_E}{2 r_e \gamma^2 N} \right)^{1/2} = 10^{-6.7} \epsilon_E \gamma_3^{-1} r_{c,9}^{1/2} (\epsilon_E N)_{29}^{-1/2} = 10^{-6.7} \epsilon_E \left[\frac{r_{c,9} \gamma_3 \Delta\nu_r f(\nu)}{S_\nu d_{\text{Gpc}}^2} \right]^{1/2}. \quad (18)$$

The nearly charge-neutral clump can radiate the total energy available in the clump but at a rate that maximizes emission in the radio band. We do not specify the mechanism that forms and holds together the clump, but it must radiate as a coherent unit long enough to produce the shot pulses with durations $\lesssim 1$ ns in the observer's frame.

5.2 Coherent Shot Pulses from Curvature Radiation

We consider radiation from a relativistic clump having net charge Q_e and Lorentz factor $\gamma \gg 1$ that comprises N particles, presumed to be electrons and positrons, produced in some short-lived, burst-like

magnetospheric event. The clump is presumed to move along a curved path (probably a particular magnetic field line), emitting curvature radiation that is optimally beamed toward the observer at some point along the path where the curvature is r_c . For notational simplicity in this section we use $\omega = 2\pi\nu$. The observed flux density is

$$S_c(\omega) \approx \frac{3^{1/3}(\omega r_c/c)^{2/3} e^2 q_c^2(\omega) \Delta\nu_r f(\xi)}{4\pi^2 d^2 c} \quad (19)$$

where, for an observer situated at an angle ϵ relative to the instantaneous plane of motion, $\xi = (\omega r_c/3c)(2\kappa_0)^{3/2} = (\omega r_c/3c)(1/\gamma^2 + \epsilon^2)^{3/2}$ and, if $\zeta = \omega r_c/3c\gamma^2$,

$$f(\xi) = \xi^{4/3} \left[K_{2/3}^2(\xi) + \left(1 - \frac{\zeta^{2/3}}{\xi^{2/3}}\right) K_{1/3}^2(\xi) \right] \quad (20)$$

(Jackson 1962); the effective squared charge of the clump is

$$q_c^2(\omega) = N + Q_c^2 F(\omega/\omega_{\text{coh}}) \quad (21)$$

where the first term arises from incoherent radiation and the second from coherent radiation. In the language of Eq. 12, the total energy radiated during the portion of the orbit where emission is directed toward the observer is $\sim \gamma^4 e^2 q_c^2(\omega)/r_c^2 c \times r_c/\gamma c \sim \gamma^3 e^2 q_c^2(\omega)/r_c$ and $f(\nu) \rightarrow f(\xi)/(\gamma^3 c/r_c)$ is the frequency spectrum; $\Delta\Omega \sim (c/\omega r_c)^{2/3}$ at frequency $\omega \lesssim \gamma^3 c/r_c$ and the fraction of the clump's energy radiated toward the observer is

$$\epsilon_E \sim \frac{\gamma^2 r_e q_c^2(\omega)}{N r_c} \approx \frac{5.9 \times 10^{-17} \gamma_3^2 q_c^2}{NP(r_c/r_{1c})}. \quad (22)$$

The form factor $F(\omega/\omega_{\text{coh}})$ is expected to be ~ 1 for coherent emission; this will be true for observed frequencies $\omega \lesssim \omega_{\text{coh}}$. Conditions for coherence are reviewed in Appendix B. For example, for a burst that lasts a time t_b and emits charges along a single field line uniformly in time over timespan t_b , $F(\omega/\omega_{\text{coh}}) = [\sin(\omega/\omega_{\text{coh}})/(\omega/\omega_{\text{coh}})]^2$, with $\omega_{\text{coh}} = 1/2t_b$. In Eq. (19) we assume that the detector bandwidth $\Delta\nu_r$ is narrow compared with the relatively broad band spectrum of instantaneous curvature radiation.

Eq. (19) implies pitifully small flux density unless coherence is substantial. Thus, we presume that $F(\omega/\omega_{\text{coh}}) \simeq 1$ for individual relativistic clump. We assume that ω_{coh} is below, but not necessarily far below, the peak frequency $\omega_{\text{pk}} = 2\pi\nu_{\text{pk}} = c\gamma^3/r_c$, where r_c is the local curvature of the charged clump path when it is beamed toward the observer:

$$\frac{\omega_{\text{coh}}}{\omega_{\text{pk}}} = \frac{\nu_{\text{coh}}}{\nu_{\text{pk}}} = \left(\frac{\gamma_{\text{coh}}}{\gamma}\right)^3 \quad \gamma_{\text{coh}} = \left(\frac{\omega_{\text{coh}} r_c}{c}\right)^{1/3} = 10^3 (P\nu_{\text{coh,GHz}})^{1/3} (r_c/r_{1c})^{1/3}, \quad (23)$$

where P is the pulsar period in seconds, and $r_{1c} = c/\Omega = cP/2\pi = 4.77 \times 10^9 P$ cm is the light cylinder radius. For comparison, the Lorentz factor required for the energy emitted in *incoherent* curvature radiation to be significant during a timescale $\delta t_e = \epsilon_t r_c/c$ (defined as a fraction ϵ_t of the characteristic time r_c/c) is

$$\gamma_{\text{incoh}} = \left(\frac{3r_c}{2r_e \epsilon_t}\right)^{1/3} = \frac{2.94 \times 10^7 P^{1/3} (r_c/r_{1c})^{1/3}}{\epsilon_t^{1/3}} = \frac{2.94 \times 10^4 \gamma_{\text{coh}}}{(\epsilon_t \nu_{\text{coh,GHz}})^{1/3}}. \quad (24)$$

The characteristic Lorentz factor associated with pulsar voltage drops is

$$\gamma_p = \frac{e\Omega^2 \mu}{2m_e c^2} = \frac{1.29 \times 10^7 \mu_{30}}{P^2}, \quad (25)$$

where $\mu = 10^{30} \mu_{30}$ G cm³ is the pulsar magnetic moment (e.g. Ruderman & Sutherland 1975).

To get a rough upper bound on the coherent emission from a single blob, we impose two constraints:

(1) coherent radiation dominates over incoherent radiation from the blob⁵ and (2) radiation losses are relatively minor during emission. To keep the treatment simple, suppose that r_c is roughly uniform along the particle path. Then the total energy radiated breaks into two pieces: the coherent part, which is from $\omega \lesssim \omega_{\text{coh}}$, where $F(\omega/\omega_{\text{coh}}) \sim 1$, and the incoherent part that arises from $\omega \sim \omega_{\text{pk}}$:

$$E_{\text{incoh}} \sim \frac{\epsilon_t N e^2 \gamma^4}{r_c} \quad E_{\text{coh}} \sim \frac{\epsilon_t Q_c^2 e^2 (\omega_{\text{coh}} r_c / c)^{4/3}}{r_c} \sim \frac{Q_c^2 E_{\text{incoh}}}{N (\omega_{\text{pk}} / \omega_{\text{coh}})^{4/3}}. \quad (26)$$

We assume that $\delta t_e \gtrsim r_c (2\kappa_0)^{1/2} / c \sim (r_c / c)^{2/3} \omega^{-1/3}$, which is the characteristic timescale *at the emitter* for radiation toward a particular observer at frequency ω , but allow for the possibility $\delta t_e \ll r_c / c$, in which case observation of the clump is highly fortuitous; consequently, with $\nu = \omega / 2\pi = 10^9 \nu_{\text{GHz}}$ GHz,

$$1 \gtrsim \epsilon_t \gtrsim \left(\frac{c}{\omega r_c} \right)^{1/3} = \frac{10^{-3}}{\nu_{\text{GHz}}^{1/3} P^{1/3} (r_c / r_{\text{lc}})^{1/3}}. \quad (27)$$

Near the lower bound, from the point of view of the observer the clump exists only for the time $\sim \omega^{-1}$ during which it emits coherently toward the observer, a doubly lucky circumstance. However, the very brightest shot pulses are rare events that may involve unusual coincidences that correspond to observational selection. Eq. (26) shows that the coherent contribution dominates if

$$\frac{Q_c^2}{N} \gtrsim \left(\frac{\omega_{\text{pk}}}{\omega_{\text{coh}}} \right)^{4/3}. \quad (28)$$

Since the total energy contained in the burst is $E_b = N \gamma m_e c^2$, then if we assume that coherent radiation dominates, radiation reaction does not severely limit the lifetime of a coherently emitting clump as long as

$$\frac{Q_c^2}{N} \lesssim \frac{\gamma m_e c^2 r_c}{\epsilon_t e^2 (\omega_{\text{coh}} r_c / c)^{4/3}} = \frac{c}{\epsilon_t \omega_{\text{coh}} r_e} \left(\frac{\omega_{\text{pk}}}{\omega_{\text{coh}}} \right)^{1/3} = \frac{1.69 \times 10^{13} (\omega_{\text{pk}} / \omega_{\text{coh}})^{1/3}}{\epsilon_t \nu_{\text{coh, GHz}}}. \quad (29)$$

Eqs. (28) and (29) are consistent with one another provided that $\gamma \lesssim \gamma_{\text{incoh}}$. Using Eq. (29) in Eq. (22) implies

$$\epsilon_E \lesssim \frac{\omega_{\text{pk}} \omega^{1/3}}{[\epsilon_t (\omega r_c / c)^{1/3}] \omega_{\text{coh}}^{4/3}} \approx \frac{10^{-3} \omega_{\text{pk}} / \omega_{\text{coh}}}{\epsilon_t (\nu_{\text{coh, GHz}} P)^{1/3}} \quad (30)$$

which is ~ 1 for ϵ_t near its lower bound according to Eq. (27).

5.3 Application to the Crab Giant Shot Pulse

In order to understand the physical requirements for this model, we investigate the conditions necessary for Eqs. (19) and (29) to account for the brightest giant pulse from the Crab pulsar. Eq. (19) requires a total charge $Q_c = 10^{21} Q_{c,21}$, where

$$Q_{c,21} = \frac{0.58 \sqrt{S_c(\omega) d^2 \Delta \nu_r^{-1} / \text{MJy kpc}^2 \text{ GHz}^{-1}}}{\nu_{\text{coh, GHz}}^{1/3} P^{1/3} (r_c / r_{\text{lc}})^{1/3} \sqrt{C(\omega / \omega_{\text{coh}}) f(\xi)}} \quad (31)$$

for coherent curvature radiation, where $C(\omega / \omega_{\text{coh}}) = (\omega / \omega_{\text{coh}})^{2/3} F(\omega / \omega_{\text{coh}})$; Eq. (29) implies

$$N \gtrsim \frac{2 \times 10^{28} \epsilon_t \nu_{\text{coh, GHz}}^{1/3} [S_c(\omega) d^2 \Delta \nu_r^{-1} / \text{MJy kpc}^2 \text{ GHz}^{-1}]}{P^{2/3} (r_c / r_{\text{lc}})^{2/3} (\omega_{\text{pk}} / \omega_{\text{coh}})^{1/3} C(\omega / \omega_{\text{coh}}) f(\xi)}, \quad (32)$$

⁵ Incoherent radiation from particles in the blob is completely different from the incoherent summation of coherent shot pulses discussed in the paper.

in agreement with the estimate in §5.2 if ϵ_t is near its lower bound in Eq. (27), and the total energy is

$$E \gtrsim \frac{1.63 \times 10^{25} \text{ ergs } \epsilon_t \nu_{\text{coh,GHz}}^{2/3} [S_c(\omega) d^2 \Delta \nu_r^{-1} / \text{MJy kpc}^2 \text{ GHz}^{-1}]}{P^{1/3} (r_c/r_{\text{lc}})^{1/3} C(\omega/\omega_{\text{coh}}) f(\xi)}. \quad (33)$$

The charge to mass ratio in the clump is therefore

$$\frac{Q_c}{N} \lesssim \frac{2.9 \times 10^{-8} P^{1/3} (r_c/r_{\text{lc}})^{1/3} (\omega_{\text{pk}}/\omega_{\text{coh}})^{1/3} \sqrt{C(\omega/\omega_{\text{coh}}) f(\xi)}}{\epsilon_t \nu_{\text{coh,GHz}}^{2/3} \sqrt{S_c(\omega) d^2 \Delta \nu_r^{-1} / \text{MJy kpc}^2 \text{ GHz}^{-1}}}; \quad (34)$$

thus, the clump must be nearly neutral, with a concentrated charge $\gtrsim 10^{21}$ to account for the brightest Crab shot pulse.

The charge per lepton in a nearly neutral clump is Q_c/N , so we expect acceleration by an electric field to result in $\gamma \simeq (Q_c/N) \gamma_p$, or

$$\frac{Q_c}{N} = \frac{\gamma_{\text{coh}}}{\gamma_p} \left(\frac{\omega_{\text{pk}}}{\omega_{\text{coh}}} \right)^{1/3} = 7.75 \times 10^{-5} P^{7/3} \mu_{30}^{-1} \nu_{\text{coh,GHz}}^{1/3} (r_c/r_{\text{lc}})^{1/3} (\omega_{\text{pk}}/\omega_{\text{coh}})^{1/3} \quad (35)$$

consistency with Eq. (34) implies

$$\frac{\epsilon_t}{(c/\omega r_c)^{1/3}} \lesssim \frac{0.377 \mu_{30} \sqrt{C(\omega/\omega_{\text{coh}}) f(\xi)}}{P^{7/3} (r_c/r_{\text{lc}})^{1/3} \nu_{\text{coh,GHz}}^{1/3} \sqrt{S_c(\omega) d^2 \Delta \nu_r^{-1} / \text{MJy kpc}^2 \text{ GHz}^{-1}}} \quad (36)$$

Eq. (36) favors fortuitously short lives for the brightest bursts, $\epsilon_t \sim (c/\omega r_c)^{1/3}$, and short spin periods.

To put the charge requirement in perspective, consider a coherent region of volume \mathcal{V}_s at radius r with density contrast C relative to the local Goldreich-Julian charge density. Then the total charge is

$$Q_c = \frac{\Omega \mu C \mathcal{V}_s}{2\pi e c r^3} \sim \frac{C \mathcal{V}_s}{2\pi e r^3} \sqrt{\frac{c I \dot{P}}{P}} = 10^{31} I_{45}^{1/2} (\dot{P}/P)_3^{1/2} (C \mathcal{V}_s / r^3) \quad (37)$$

where $I = 10^{45} I_{45} \text{ g cm}^2$ is the stellar moment of inertia and $\dot{P}/P = (\dot{P}/P)_3 / 10^3 \text{ y}$. For the Crab's largest giant (shot) pulse $C \mathcal{V}_s / r^3 \sim 10^{-10}$, or $(C \mathcal{V}_s)^{1/3} \sim 15 (r/10 \text{ km})$ light-nanoseconds = $2.4 (r/r_{\text{lc}})$ light-microseconds, which are both larger than $c/\nu \sim$ light-nanoseconds. Appendix B shows that coherently emitting volumes can be far larger than $(c/\nu)^3$. Eq. (B7) implies volumes $\mathcal{V}_s \sim \gamma^3 (c/\nu)^3$, or $\mathcal{V}_s^{1/3} \sim \gamma c/\nu = \gamma_3 / \nu_{\text{GHz}}$ light-microseconds, which is close to what is necessary for the Crab's largest giant (shot) pulse if it originated near the light cylinder.

The energy requirement, Eq. (33), is impossible to assess without a detailed model for the formation and acceleration of a clump. A standard of comparison for the clump energy in Eq. (33) is the total magnetic energy in the unperturbed volume $C \mathcal{V}_s$ near radius r i.e.

$$E_B(r) = \frac{\mu^2 C \mathcal{V}_s}{8\pi r^6} \sim \frac{I (\dot{P}/P) C \mathcal{V}_s}{4P (r/r_{\text{lc}})^3 r^3} = \frac{7.9 \times 10^{33} \text{ ergs } (\dot{P}/P)_3 (C \mathcal{V}_s / r^3)}{P (\Omega r / c)^3}. \quad (38)$$

For the Crab, Eq. (38) implies $E_B(r_{\text{lc}}) \sim 2 \times 10^{25} \text{ ergs}$ for $(C \mathcal{V}_s / r^3) \sim 10^{-10}$, which is comparable to Eq. (33), particularly if ϵ_t is near the lower bound implied by Eq. (27).

This concordance suggests that the flux density of the brightest Crab pulsar giant pulse is near the maximum that can be produced near the pulsar's light cylinder. Eq. (38) could permit flux densities larger than $\sim \text{MJy}$ if the coherent emission arises somewhat (but not very far) inside the light cylinder: Eq. (33) implies an energy bound proportional to the flux density, whereas Eq. (38) suggests an energy reservoir $\propto r^{-6}$ at a fixed value of $C \mathcal{V}_s / r_{\text{lc}}^3$. In view of the statistical considerations in Section 3.3, this concordance suggests that the high S tail of the PDF of giant pulse flux densities for the Crab pulsar is relatively shallow.

5.4 Application to Bursts from Extragalactic Neutron Stars

A 1 Jy burst lasting 1 ms from a source at 1 Gpc distance corresponds to a luminosity $\mathcal{L}_\nu = 1 \text{ Jy Gpc}^2 \text{ ms} = 10^{12} \text{ MJy kpc}^2 \text{ GHz}^{-1}$ in the observational frequency band. In the curvature radiation model, \mathcal{L}_ν determines the total charge squared, Q_b^2 , associated with the burst; $Q_b^2 = N_i \langle Q_c^2 \rangle$ for a burst consisting of N_i incoherently-summed shot pulses with mean square charge $\langle Q_c^2 \rangle$ per coherently-emitting shot pulse. Scaling from Eqs. (31) and (33) we find

$$\begin{aligned} Q_b &= \frac{5.8 \times 10^{26} \sqrt{\mathcal{L}_\nu / \text{Jy Gpc}^2 \text{ ms}}}{\nu_{\text{coh, GHz}}^{1/3} P^{1/3} (r_c / r_{\text{lc}})^{1/3} \sqrt{C(\omega / \omega_{\text{coh}}) f(\xi)}} \\ E &\gtrsim \frac{1.63 \times 10^{37} \text{ ergs } \epsilon_t \nu_{\text{coh, GHz}}^{2/3} (\mathcal{L}_\nu / \text{Jy Gpc}^2 \text{ ms})}{P^{1/3} (r_c / r_{\text{lc}})^{1/3} C(\omega / \omega_{\text{coh}}) f(\xi)}. \end{aligned} \quad (39)$$

Eqs. (39) do not depend on N_i : they follow from the total luminosity of the burst.

If \mathcal{V}_i is the volume occupied by the incoherently superposed clumps, then the characteristic charge and energy reservoirs associated with this region are given by Eqs. (37) and (38) with the replacement $C\mathcal{V}_s \rightarrow \mathcal{V}_i$:

$$\begin{aligned} Q_i &= \frac{\Omega \mu \mathcal{V}_i}{2\pi e c r^3} \sim \frac{\mathcal{V}_i}{2\pi e r^3} \sqrt{\frac{c I \dot{P}}{P}} = 10^{31} I_{45}^{1/2} (\dot{P}/P)_3^{1/2} (\mathcal{V}_i / r^3) \\ E_B(r) &= \frac{\mu^2 \mathcal{V}_i}{8\pi r^6} \sim \frac{I(\dot{P}/P) \mathcal{V}_i}{4P(r/r_{\text{lc}})^3 r^3} = \frac{7.9 \times 10^{33} \text{ ergs } (\dot{P}/P)_3 (\mathcal{V}_i / r^3)}{P(r/r_{\text{lc}})^3}. \end{aligned} \quad (40)$$

Superficially, the first of Eqs. (39) is well within the charge reservoir Q_i , thus allowing \mathcal{V}_i / r^3 to be small. However, recall that Q_b^2 is the *total squared charge* for N_i clumps, so if all of the Q_c have the same sign then the total charge involved in the outburst is $\sim Q_b \sqrt{N_i}$, which would almost certainly exceed the available charge Q_i even if $\mathcal{V}_i / r^3 \sim 1$. Curvature radiation for individual clumps does not depend on the sign of their charges, though, and this difficulty is avoided if positive and negative Q_c are equally likely, in which case the expected net charge would be $\sim \pm Q_c \sqrt{N_i} \sim \pm Q_b$.

The energy required by the second of Eqs. (39) is harder to reconcile with Eq. (40); taken together they require

$$\frac{\mathcal{L}_\nu}{\text{Jy Gpc}^2 \text{ ms}} \lesssim \frac{1.6 I_{45} (\dot{P}/P)_3 (r_c / r_{\text{lc}})^{2/3} \nu_{\text{GHz}}^{1/3} C(\omega / \omega_{\text{coh}}) f(\xi)}{(P/30 \text{ ms})^{1/3} [\epsilon_t (\omega r_c / c)^{1/3}] \nu_{\text{coh, GHz}}^{2/3}} \left(\frac{\mathcal{V}_i r_{\text{lc}}^3}{r^6} \right), \quad (41)$$

where we have adopted the most favorable case in which outbursts are associated with the first ~ 1000 years of a pulsar's life, when it might be expected to resemble the Crab pulsar. Eq. (41) favors (i) small $\epsilon_t \simeq (c/\omega r_c)^{1/3}$, its minimum value, (ii) large \dot{P}/P , (iii) short P and (iv) comparatively small distances,

$$d_{\text{Gpc}} \sqrt{\frac{S_{\nu, \text{th}} W_i}{\text{Jy ms}}} \lesssim \frac{1.2 I_{45}^{1/2} (\dot{P}/P)_3^{1/2} (r_c / r_{\text{lc}})^{1/3} \nu_{\text{GHz}}^{1/6} \sqrt{C(\omega / \omega_{\text{coh}}) f(\xi)}}{(P/30 \text{ ms})^{1/6} [\epsilon_t (\omega r_c / c)^{1/3}]^{1/2} \nu_{\text{coh, GHz}}^{1/3}} \left(\frac{\mathcal{V}_i r_{\text{lc}}^3}{r^6} \right)^{1/2} \quad (42)$$

where $S_{\nu, \text{th}}$ is the detection threshold. If we estimate $\mathcal{V}_i \simeq (cW_i)^3$ then $\mathcal{V}_i / r_{\text{lc}}^3 \simeq (\Omega W_i)^3 = 9.2 \times 10^{-3} [W_{i, \text{ms}} / (P/30 \text{ ms})]^3$. Using this as a benchmark value in Eq. (42) implies

$$d_{\text{Gpc}} \sqrt{\frac{S_{\nu, \text{th}} W_i}{\text{Jy ms}}} \lesssim \frac{0.11 W_{i, \text{ms}}^{3/2} I_{45}^{1/2} (\dot{P}/P)_3^{1/2} (r_c / r_{\text{lc}})^{1/3} \nu_{\text{GHz}}^{1/6} \sqrt{C(\omega / \omega_{\text{coh}}) f(\xi)}}{(P/30 \text{ ms})^{5/3} [\epsilon_t (\omega r_c / c)^{1/3}]^{1/2} \nu_{\text{coh, GHz}}^{1/3}} \left[\frac{\mathcal{V}_i r_{\text{lc}}^3}{r^6 (\Omega W_i)^3} \right]^{1/2} \quad (43)$$

Eq. (43) depends sensitively on P and r , and less sensitively on \dot{P}/P . Pulsars younger and faster spinning than the Crab pulsar would be visible to larger distances: for $(\dot{P}/P)_3^{1/2} (P/30 \text{ ms})^{-5/3} (r_{\text{lc}}/r)^3 \simeq 10$

the limiting distance implied by Eq. (43) is $\simeq 1$ Gpc. However, “ordinary” pulsars with $\dot{P}/P = 10^{-7}(\dot{P}/P)_7 \text{yr}^{-1}$ are visible to $\sim 3(\dot{P}/P)_7^{1/2} P^{-5/3} (r_{\text{lc}}/r)^3$ kpc, where P is in seconds. This is within the Galaxy for $r_{\text{lc}}/r \simeq 1$, and to be visible at $\simeq 1$ Gpc emission would have to originate at $r/r_{\text{lc}} \lesssim 0.01$. Single pulses with amplitude ~ 0.2 Jy and widths ~ 20 ms have been seen from pulsar J0529–6652 ($P = 975$ ms, $\dot{P}/P \sim 5 \times 10^{-5} \text{yr}^{-1}$) in the Large Magellanic cloud with $d = 54$ kpc (Crawford et al. 2013). Magnetars have $(\dot{P}/P)_3 \sim 0.01 - 1$ and $P \sim 1 - 10$ seconds, and would therefore be visible to $\lesssim 300(\dot{P}/P)_3^{1/2} P^{-5/3} (r_{\text{lc}}/r)^3$ kpc, normalizing to the *most favorable* values of \dot{P}/P and P ; for $r_{\text{lc}}/r \simeq 1$ this limiting distance is well within the Local Group, and for typical magnetar parameters, within the Galaxy. For detection to $\simeq 1$ Gpc radiation would have to originate at $r/r_{\text{lc}} \lesssim 0.01 - 0.1$.

Henceforth, we tentatively assume that the coherently emitting clumps that comprise an ERB resemble the clump that caused the Crab’s largest giant shot pulse, and use the properties we have inferred for it to consider other constraints.

5.5 Radiation Drag

The clump experiences drag by ambient radiation in addition to the “radiation reaction drag” it experiences by interactions with its own radiation field. The drag force depends on how opaque the clump is, which requires us to model its shape, but at a given N an upper bound is found by assuming that the clump is optically thin, which implies that the clump loses energy via drag at a rate $-\dot{E}_{\text{drag}} \lesssim N\gamma^2 c\sigma_T f(k)U_{\text{rad}}$, where U_{rad} is the ambient radiation energy density in the inertial frame where the clump moves relativistically. The factor $f(k)$ depends on the characteristic photon energy $km_e c^2$ in the rest frames of scattering leptons in the clump: $f(k) < 1$ in general, $f(0) = 1$ and $f(k) \simeq 3 \ln(2k)/8k$ for $k \gg 1$ (e.g. Jauch & Rohrlich 1976). Since the clump has energy $N\gamma m_e c^2$, the drag lifetime is t_{drag} , where

$$\frac{ct_{\text{drag}}}{r_c} \gtrsim \frac{m_e c^2}{\gamma r_c \sigma_T f(k) U_{\text{rad}}} = \frac{5.61 \times 10^4 (\omega_{\text{coh}}/\omega_{\text{pk}})^{1/3} P^{11/3}}{\nu_{\text{coh,GHz}}^{1/3} (r_c/r_{\text{lc}})^{4/3} I_{45} \dot{P}_{15} (f(k) U_{\text{rad}}/U_{\text{lc}})}; \quad (44)$$

we estimated U_{rad} by $U_{\text{lc}} = I\Omega\dot{\Omega}/4\pi r_{\text{lc}}^2 c = 4\pi^3 I \dot{P}/c^3 P^5 = 4.59 I_{45} \dot{P}_{15} P^{-5} \text{erg cm}^{-3}$, where $I = 10^{45} I_{45} \text{g cm}^2$ is the moment of inertia of the neutron star, and $\dot{P} = 10^{-15} \dot{P}_{15}$ is the spin-down rate. Although Eq. (44) suggests that drag is unimportant for nominal parameter values, this may be deceptive in specific cases: for Crab pulsar parameters, Eq. (44) implies

$$\frac{ct_{\text{drag}}}{r_c} \gtrsim \frac{5 \times 10^{-4} (\omega_{\text{coh}}/\omega_{\text{pk}})^{1/3}}{\nu_{\text{coh,GHz}}^{1/3} (r_c/r_{\text{lc}})^{4/3} I_{45} f(k) (U_{\text{rad}}/U_{\text{lc}})} \quad [\text{Crab}] \quad (45)$$

suggesting a short lifetime: for comparison, $\epsilon_t \gtrsim 3 \times 10^{-3} \nu_{\text{GHz}}^{-1/3} (r_c/r_{\text{lc}})^{-1/3}$ for the Crab according to Eq. (27), comparable to but larger than Eq. (45). The mild discrepancy may be resolved if the clump is moderately opaque even if $k \ll 1$; and the drag timescale is considerably longer – perhaps even $\sim r_c/c$ – if $k \gg 1$.

Within the larger volume \mathcal{V}_i , coherent regions can interact with one another via their radiation fields. If $W_i \sim 1$ ms and the radiation-reaction lifetimes of clumps are $r_c/c\gamma \simeq 0.15P/\gamma_3$ ms (i.e. near the small end of Eq. (27) then the radiation energy density within \mathcal{V}_i during the lifetime of a particular coherently emitting clump is within an order of magnitude of the total energy emitted during the burst. The radiation density is in the form of a concentrated beam of energy directed toward the observer. This directed energy would accelerate the clumps. A detailed calculation of this effect requires more specific modelling of the overall emission event, and we do not attempt it here.

5.6 Pair Annihilation

Since the clump consists of N electrons and positrons with a relatively small net excess of one charge $Q_c \ll N$ its lifetime may also be limited by e^\pm annihilation. If n_{rf} is the pair density in the rest frame of the clump, then the annihilation rate per volume, a Lorentz scalar, is $\sim n_{\text{rf}}^2 (\sigma v)_{\text{ann}}$, where $(\sigma v)_{\text{ann}} \approx \pi e^4 A(\gamma_{\text{int}}) / m_e^2 c^3 = \frac{3}{8} \sigma_T c A(\gamma_{\text{int}})$ is the pair annihilation rate coefficient for relative motion with Lorentz factors γ_{int} , where $A(1) = 1$ and $A(\gamma_{\text{int}}) \simeq \ln \gamma_{\text{int}} / \gamma_{\text{int}}^2$ for $\gamma_{\text{int}} \gg 1$ (e.g. Jauch & Rohrlich 1976). (We assume that the clump is hot enough in its rest frame that we can neglect annihilation via the formation of positronium.) Then Lorentz transform to the inertial frame of the magnetosphere, where the density is $n_b = \gamma n_{\text{rf}}$, to get the annihilation rate per lepton, $n_b (\sigma v)_{\text{ann}} / \gamma^2$, implying a lifetime t_{ann} , where

$$\frac{ct_{\text{ann}}}{r_c} = \frac{\gamma^2 c}{n_b r_c (\sigma v)_{\text{ann}}} \sim \frac{8\gamma^2 (c/\omega_{\text{coh}} r_c)}{3\tau_b A(\gamma_{\text{int}})} \gtrsim \frac{8(\omega_{\text{coh}} r_c / c)^{2/3} (\omega_{\text{pk}} / \omega_{\text{coh}})^{2/3}}{3\tau_b} \quad (46)$$

where τ_b is the Thomson optical depth of the clump and the length of the clump along its direction of motion is $\sim c/\omega_{\text{coh}}$. The lifetime of the clump against pair annihilation is long compared with its drag and radiation reaction lifetimes.

5.7 Conjectures on Clumping Mechanisms

A possible mechanism for the formation of the relativistic clump responsible for the sub-bursts is the bunching instability associated with coherent synchrotron radiation. There has not yet been a treatment of this instability that made specific reference to a nearly neutral system with e^\pm pairs: analyses done to date (Goldreich & Keeley 1971; Schmekel et al. 2005; Schmekel & Lovelace 2006) considered configurations of relativistic electrons only. Linear growth rates found in these treatments appear to be fast enough to initiate the instability on timescales much shorter δt_e on small length scales. However, we have seen that coherent emission requires a large number of leptons confined to a small volume, leading to extremely large density contrast relative to the GJ density; thus a nonlinear analysis is needed to establish that this mechanism is viable. Another possible mechanism for generating dense clumps is the two stream instability (e.g. Ruderman & Sutherland 1975; Benford & Buschauer 1977; Buschauer & Benford 1978). Magnetospheric reconnection events conceivably may play a role by producing relativistic charge streams or could trigger secondary activity (e.g. pair production) that leads to giant bursts.

6 EXTRAGALACTIC POPULATIONS OF NEUTRON STARS

Extragalactic NS formed over cosmological time are potential sources of super-strong bursts that occur only rarely per object. We associate the burst rate with the cosmological birth rate of NS, each object emitting a small number of detectable bursts, $N_b = \eta_b T_b$, at a low rate η_b in a burst phase of duration T_b . A more detailed calculation could include separate birth and burst rates, but the net result is the same. We use the Galactic rate of NS formation per unit stellar mass, $\dot{n}_{\text{ns,M}} \approx \dot{n}_{\text{ns,M,-13}} 10^{-13} \text{ yr}^{-1} M_\odot^{-1}$ (e.g. one NS every 100 yr per $10^{11} M_\odot$ in stars) in combination with the average stellar mass density $\rho_* = \Omega_* \rho_c$ to calculate the aggregate NS birth and ERB burst rates, where $\rho_c = 3H_0^2 / 8\pi G$ is the closure density and $\Omega_* \approx 0.003 \Omega_{*,0.003}$ (Read & Trentham 2005).

About $N_{\text{ns}} \sim 10^{17}$ NS are produced in a Hubble volume $V_H = 4\pi d_H^3 / 3$ for a Hubble distance $d_H = c/H_0 = 4.3 h_{0.7}^{-1} \text{ Gpc}$ and a typical galaxy age $T_{\text{gal}} = 10 \text{ Gyr}$. The aggregate NS birth rate scaled from the local rate in the Galaxy,

$$\Gamma_{\text{ns}} = \rho_c \Omega_* \dot{n}_{\text{ns,M}} V_H \sim 4 \times 10^4 \text{ day}^{-1} h_{0.7}^{-1} \dot{n}_{\text{ns,M,-13}} \Omega_{*,0.003}, \quad (47)$$

is tantalizingly similar to the inferred ERB burst rate $\Gamma_{\text{b,obs}} \approx 10^3\text{-}10^4 \text{ day}^{-1}$ (Thornton et al. 2013;

Spitler et al. 2014; Law et al. 2015; Keane & Petroff 2015), suggesting that only of order one burst per NS is needed to account for ERBs. Larger N_b would allow a nearer population with $d_{\max} \ll d_H$.

In the following we estimate ERB rates by including beaming of radiation and a redshift-dependent star formation rate (SFR). We assume that beaming toward Earth is favorable for a fraction $f_b = 0.1 f_{b,0.1}$ of the bursts that are bright enough to be detectable throughout the relevant volume. Values of f_b for pulsars are similar but depend on spin period and on the emission being steady as the beam rotates across the sky. ERBs could have substantially smaller f_b if burst durations are a purely temporal phenomenon in a frame rotating with the pulsar. However, the beaming fraction for f_b can be comparable to that of pulsars if pulse widths are mostly due to beam rotation. The aggregate burst rate per unit volume is then $d\Gamma_b/d(\text{vol}) = f_b N_b \dot{n}_{\text{ns},M} \rho_\star$.

6.1 Implications of Non-detections in Followup Observations

Individual ERB fields have been reobserved for up to ~ 40 hr, yielding no repeat bursts (Lorimer et al. 2007) but providing identification of one new ERB (Petroff et al. 2015a,b). One conclusion that can be made is that the population is extragalactic. This may be seen by calculating the burst rate *per NS* as a function of maximum population distance, $\eta_b = \Gamma_{\text{b,obs}}(d_H/d_{\max})^3 / f_b \Gamma_{\text{ns}} T_{\text{gal}}$. To have $\eta_b \lesssim 1 \text{ d}^{-1}$ requires $d_{\max} \gtrsim 0.4$ Mpc. However, if bursts are associated with a special phase in a NS's lifetime, the available subset of NS is much smaller, requiring more bursts per NS and accordingly a larger maximum distance to avoid any repeats.

The lack of redetections also provides constraints on the burst rate per source η_b depending on assumptions about the pulse-amplitude PDF. For simplicity here, we assume that all bursts have the same intrinsic luminosity and can be detected out to some maximum distance d_{\max} (also discussed as Case I in Section 6.3.1). The sky density of such sources is n_Ω sources deg^{-2} .

Let Ω_{FoV} be the solid angle of the telescope field of view (FoV) for a single pointing and consider a total followup time T_F for an individual sky position. Assuming many ERB sources are within the FoV, $f_b n_\Omega \Omega_{\text{FoV}} \gg 1$, where f_b is the beaming factor, as above, the mean number of detected bursts is

$$\langle N_{\text{ERB}} \rangle = \eta_b T_F (f_b n_\Omega \Omega_{\text{FoV}}). \quad (48)$$

If sources are sparsely distributed on the sky (or highly clustered) so that only the originally detected ERB source is within the FoV, $f_b n_\Omega \Omega_{\text{FoV}}$ would be replaced by unity, so generally $\langle N_{\text{ERB}} \rangle = \eta_b T_F \max(1, f_b n_\Omega \Omega_{\text{FoV}})$. With no redetections, $\langle N_{\text{ERB}} \rangle \ll 1$ and the limit on the rate is

$$\eta_b \ll \frac{1}{T_F \max(1, f_b n_\Omega \Omega_{\text{FoV}})}, \quad (49)$$

which shows that the rate per source derived from reobservations needs to take into account the sensitivity to *all* ERB sources in the FoV that are sampled simultaneously, not just the source of the original ERB.

The number of extragalactic NS in the FoV of any single-dish telescope is very large. With $N_{\text{NS}} \sim 10^{17}$ NS in a Hubble volume, the sky density for $d_{\max} = 1 \text{ Gpc}$ d_{Gpc} is

$$n_\Omega = \frac{N_{\text{NS}}}{4\pi} \left(\frac{d_{\max}}{d_H} \right)^3 \approx 3 \times 10^{10} d_{\text{Gpc}}^3 \text{ deg}^{-2}. \quad (50)$$

To have only a single ERB source in a 1 deg^{-2} FoV would imply a local population of NS with a very small population distance,

$$d_{\max} \leq 0.7 \text{ Mpc} h_{0.7}^{-1} (f_{b,0.1} \Omega_{\text{FoV,deg}^2})^{-1/3}, \quad (51)$$

which is inconsistent with the sky locations of ERBs seen to date. The implied rate per ERB is therefore

very small for reobservations done so far,

$$\eta_b \ll 3 \times 10^{-7} \text{ hr}^{-1} (f_{b,0.1} T_{F,\text{hr}} \Omega_{\text{FoV,deg}^2})^{-1} d_{\text{Gpc}}^{-3}, \quad (52)$$

even taking into account $\Omega_{\text{FoV}} \sim 0.06 \text{ deg}^2$ for a single beam of the Parkes telescope, which is nearly cancelled by $T_F \sim$ tens of hours reobservation times. The very small rate limit is completely consistent with the statement that only a small number of bursts is needed per NS if the population extends to Gpc distances.

6.2 Low-redshift Population

For a local (low-redshift) population, the burst rate for a maximum population distance d_{max} is $\Gamma_b(d_{\text{max}}) = \Gamma_{b,H} (d_{\text{max}}/d_H)^3$, where the local burst rate is normalized to a Hubble volume,

$$\Gamma_{b,H} = f_b N_b \Gamma_{\text{ns}} = \frac{c^3 f_b N_{b0} \dot{n}_{\text{ns},M,0} \Omega_{\star,0}}{2H_0 G} \approx 4 \times 10^3 \text{ day}^{-1} f_{b,0.1} N_b \left(\frac{\Gamma_{\text{ns}}}{4 \times 10^4 \text{ day}^{-1}} \right). \quad (53)$$

To match $\Gamma_b(d_{\text{max}})$ with $\Gamma_{b,\text{obs}}$ requires

$$N_b = \frac{\Gamma_{b,\text{obs}}}{f_b \Gamma_{\text{ns}}} \left(\frac{d_H}{d_{\text{max}}} \right)^3 \approx \frac{200}{f_{b,0.1} d_{\text{max,Gpc}}^3} \left(\frac{\Gamma_b}{10^4 \text{ day}^{-1}} \right) \left(\frac{4 \times 10^4 \text{ day}^{-1}}{\Gamma_{\text{ns}}} \right). \quad (54)$$

Even for a relatively nearby population with $d_{\text{max}} = 100 \text{ Mpc}$, the number of bursts per object, $N_b \approx 2 \times 10^5$, is a small fraction of the total number of turns of a NS in its lifetime, whether defined as the giant-pulse emitting time span, the total radio-emitting span, or the age of the NS itself. In time T_b the number of turns is $\phi_T \sim \dot{P}_0^{-1} (T_b/\tau_0)^{(n-2)/(n-1)}$ for a starting period P_0 and period derivative \dot{P}_0 , yielding a spindown time $\tau_0 = P_0/(n-1)\dot{P}_0$ for a braking index n . The Crab pulsar will make $\sim 10^{12}$ turns in the next 10^3 yr and 10^{14} turns in 10^9 yr assuming a constant braking index. If ERBs are similar to giant pulses emitted in the first $T_b = 10^3 \text{ yr}$ of a NS, the interval between ERBs per object is only tens to hundreds of hours. However, rare events occurring at any point in the lifetime of a NS (e.g. $\gtrsim 1 \text{ Gyr}$) imply intervals of tens to hundreds of years or longer.

The number of bursts per source is tied to the contributions of the IGM and any host galaxy to the observed DMs of ERBs. If the maximum population distance is of order d_H , the IGM can and must account for nearly all the excess over the Milky Way's contribution. Conversely, a nearby $\sim 100 \text{ Mpc}$ (or closer) population requires a dominant contribution from host galaxies, in particular from dense star-forming regions or galactic centres.

6.3 High-redshift Population

For populations extending to high redshifts, we relate the local NS birth rate $\dot{n}_{\text{ns},M}(z)$ to the SFR $\psi(z)$ (in standard units $M_\odot \text{ yr}^{-1} \text{ Mpc}^{-3}$; e.g. Madau & Dickinson 2014)

$$\dot{n}_{\text{ns},M\rho_\star}(z) = \nu_{\text{ns}}(z)\psi(z) \quad (55)$$

where $\nu_{\text{ns}}(z)$ is the number of neutron stars per stellar mass formed at redshift z and the stellar mass density is a co-moving density. Using the beaming fraction, assumed independent of z , and the number of bursts per NS, $N_b(z)$, now possibly redshift dependent, the burst rate out to a maximum redshift z_{max} is

$$\Gamma_b(\leq z_{\text{max}}) = 4\pi f_b \int_0^{z_{\text{max}}} dz \frac{dr(z) r^2(z) N_b(z) \nu_{\text{ns}}(z) \psi(z)}{(1+z)}. \quad (56)$$

where $r(z)$ is the comoving radial coordinate and $4\pi dz r^2(z) dr(z)/dz$ is the comoving volume element. The $1+z$ factor in the denominator accounts for the redshift of the NS birth rate.

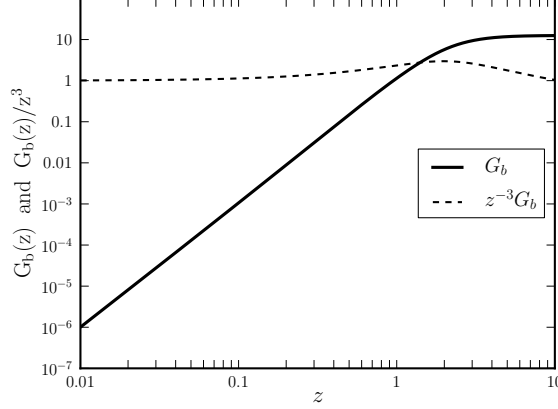


Figure 3. Volume integral $G_b(z)$ for bursts in a Λ CDM cosmology with $\Omega_M = 0.27$ for the case where the number of bursts per source N_b is independent of z ;

By normalizing $\nu_{ns}(z)$ and $\psi(z)$ to local values,

$$\nu_{ns}(z) = \nu_{ns}(0)\hat{\nu}_{ns}(z) \quad \text{and} \quad \psi(z) = \psi(0)\hat{\psi}(z), \quad (57)$$

the rate becomes

$$\Gamma_b(\leq z_{\max}) = 4\pi f_b \dot{n}_{ns, M, 0} \rho_{\star}(0) \int_0^{z_{\max}} dz \frac{dr_c(z) [r_c(z)]^2 N_b(z) \hat{\nu}_{ns}(z) \hat{\psi}(z)}{1+z}. \quad (58)$$

6.3.1 Case I: Constant N_b vs. z

One possibility is that ERBs are associated with extremely rare, triggered events occurring N_b times during the lifetime of a NS. If bright enough intrinsically – e.g. flux densities $\gtrsim 10^{12}$ Jy at a fiducial kpc distance – such events could be detectable at cosmological distances, up to some cutoff $z_c \gtrsim 1$. In this case $N_b(z)$ is independent of z since it is determined entirely by activity internal to the NS or in the magnetosphere, or to external triggers that do not involve redshift-dependent conditions. In general, $\nu_{ns}(z)$ depends on the initial mass function (IMF), which depends on z . However, at modest $z \lesssim 1$ (but not $z \gg 1$) it is also plausible that it is close to the local value and therefore $\hat{\nu}_{ns}(z) = 1$. Under these circumstances we write the burst rate in terms of a dimensionless integral $G_b(z)$ over the normalized SFR, $\hat{\psi}(z)$,

$$\Gamma_b(\leq z_{\max}) = \Gamma_{b,H} G_b(z_{\max}), \quad \text{with} \quad G_b(z) = 3 \int_0^z dz' \frac{d\tilde{r}(z')}{dz'} \frac{\tilde{r}^2(z') \hat{\psi}(z')}{1+z'}. \quad (59)$$

The dimensionless radial coordinate is $\tilde{r}(z) = \int_0^z dz'/E(z')$ where $E(z) = \sqrt{1 - \Omega_M + \Omega_M(1+z)^3}$ for a Λ CDM cosmology with a fractional matter density Ω_M .

To obtain $G_b(z)$ we use the empirical fit to the cosmological SFR (Madau & Dickinson 2014, Eq. 15),

$$\psi(z) = \frac{0.015(1+z)^{2.7}}{1 + [(1+z)/2.9]^{5.6}} M_{\odot} \text{ yr}^{-1} \text{ Mpc}^{-3}, \quad (60)$$

and normalize it to $z = 0$ to get $\hat{\psi}(z)$.

Figure 3 shows $G_b(z)$. For low maximum redshifts, $G_b(z) \approx z^3$ so the ratio $G_b(z)/z^3$, also shown in the figure, is unity as expected. At high maximum redshifts $G_b(z)$ flattens to a value ~ 10 times the

value at $z = 1$, indicating that a very distant population would not require all NS to contribute to observed ERBs⁶.

6.3.2 Case II: $N_b(z)$ for an Intrinsic Distribution of Burst Luminosities

In actuality, $N_b(z)$ is determined by the number of bursts per pulsar bright enough to be detected to redshift z via observations at frequency ν . This involves the distribution of intrinsic burst luminosities, \mathcal{L}_ν (with units of luminosity per unit frequency). We express the number of bursts with luminosities above \mathcal{L}_ν as $\mathcal{N}_b(> \mathcal{L}_\nu)$.

The key is detectability: we suppose that a burst will be detected with a flux density threshold $S_{\nu,\text{th}}$ over a timescale W_i ; we define $A_\nu^{(\text{th})} = S_{\nu,\text{th}}W_i$. For a source at redshift z , we refer the threshold luminosity to the observational frequency, so the $\mathcal{L}_\nu^{(\text{th})}$ involves both an appropriate redshift-dependent distance and a color correction; we find

$$\mathcal{L}_\nu^{(\text{th})} = \frac{P(\nu)d_L^2(z)A_\nu^{(\text{th})}}{(1+z)P(\nu(1+z))} = \frac{P(\nu)(1+z)r^2(z)A_\nu^{(\text{th})}}{P(\nu(1+z))} = \frac{P(\nu)(1+z)\tilde{r}^2(z)\mathcal{L}_{\nu,H}^{(\text{th})}}{P(\nu(1+z))} \quad (61)$$

for a source at redshift z , where $P(\nu)$ is the spectrum; $d_L(z) = (1+z)r_c(z)$ is the luminosity distance where $r_c(z) = d_H\tilde{r}(z)$ is the radial coordinate to the source, and

$$\mathcal{L}_{\nu,H}^{(\text{th})} = A_\nu^{(\text{th})}d_H^2 = \frac{18.4 \text{ Jy ms Gpc}^2}{h_{0.7}^2} \left(\frac{A_\nu^{(\text{th})}}{1 \text{ Jy ms}} \right) = \frac{18.4 \times 10^{12} \text{ MJy ns kpc}^2}{h_{0.7}^2} \left(\frac{A_\nu^{(\text{th})}}{1 \text{ Jy ms}} \right) \quad (62)$$

where $d_H = c/H_0 = 4.29h_{0.7}^{-1} \text{ Gpc}$ for $H_0 = 70h_{0.7} \text{ km s}^{-1} \text{ Mpc}^{-1}$. For coherent curvature radiation, $P(\nu) \propto \nu^{2/3}$ below a cutoff frequency ν_c above which the spectrum cuts off exponentially so we approximate

$$f(z) = \frac{P(\nu)(1+z)\tilde{r}^2(z)}{P(\nu(1+z))} \simeq \tilde{r}^2(z)(1+z)^{1/3}e^{\nu z/\nu_c} \equiv \tilde{r}^2(z)(1+z)^{1/3}e^{z/z_c} \quad (63)$$

where we bear in mind that $z_c \equiv \nu_c/\nu$ depends on the observational frequency ν . Notice that $f(z)$ is an increasing function of z : as z increases, the sources that we can detect have ever increasing intrinsic luminosities. With these definitions,

$$N_b(z) = \mathcal{N}_b(> \mathcal{L}_{\nu,H}^{(\text{th})} f(z)), \quad (64)$$

which can be inserted into Eq. (58).

Eq. (58) integrates the rate to z_{max} . Via energetic arguments, we have shown that there is an upper luminosity cutoff $\mathcal{L}_{\nu,u}$ to the distribution of bursts. Consequently, for a given observational survey, z_{max} is determined by solving $\mathcal{L}_{\nu,u} = \mathcal{L}_{\nu,H}^{(\text{th})} f(z_{\text{max}})$. There is also a minimum burst luminosity, $\mathcal{L}_{\nu,l}$, although its definition may be problematic because it involves qualitative criteria for distinguishing an outburst from “normal fluctuations” in pulsar luminosity. Nevertheless, there is also a maximum redshift z_l to which we can observe the faintest outburst, which is determined by $\mathcal{L}_{\nu,l} = \mathcal{L}_\nu^{(\text{th})} f(z_l)$; all outbursts are detectable out to z_l , but only sufficiently luminous ones are detectable for $z_l < z \leq z_{\text{max}}$. Thus, the observed burst rate is

$$\Gamma_b(\leq z_{\text{max}}(S_{\nu,\text{th}})) = f_b \Gamma_{\text{ns}} \left[N_{b,\text{total}} G_b(z_l(S_{\nu,\text{th}})) + \int_{z_l(S_{\nu,\text{th}})}^{z_{\text{max}}(S_{\nu,\text{th}})} dz \frac{dG_b(z)}{dz} \mathcal{N}_b(> \mathcal{L}_{\nu,H}^{(\text{th})} f(z)) \right], \quad (65)$$

⁶ Dispersion measures of ERBs indicate redshifts $z < 1$ if the IGM is smoothly distributed. The clumpiness of the cosmic web may allow more distant objects to be seen with the measured DMs (Lorimer et al. 2007; Thornton et al. 2013; Spitler et al. 2014). However, scattering in the IGM or radiation physics may not allow bursts from such sources to be detectable.

where $N_{b,\text{total}}$ is the *mean* total number of outbursts per pulsar brighter than $\mathcal{L}_{\nu,l}$. Presumably there is a distribution of $N_{b,\text{total}}$ that depends on pulsar properties, but we assume that this distribution does not vary with z . The observed bursts will be dominated by the intrinsically *brightest* bursts if $\mathcal{N}_b(> \mathcal{L}_\nu)$ is *shallow*, and by the intrinsically *faintest* bursts if it is *steep*. Given the uncertainty in $\mathcal{N}_b(> \mathcal{L}_\nu)$, we define an effective number of bursts per pulsar as a function of z_{max} via $\Gamma_b(\leq z_{\text{max}}) \equiv f_b \Gamma_{\text{ns}} N_{b,\text{eff}}(z_{\text{max}}) G_b(z_{\text{max}})$, or

$$N_{b,\text{eff}}(z_{\text{max}}(S_{\nu,\text{th}})) = \frac{1}{G_b(z_{\text{max}}(S_{\nu,\text{th}}))} \left[N_{b,\text{total}} G_b(z_l(S_{\nu,\text{th}})) + \int_{z_l(S_{\nu,\text{th}})}^{z_{\text{max}}(S_{\nu,\text{th}})} dz \frac{dG_b(z)}{dz} \mathcal{N}_b(> \mathcal{L}_{\nu,H}^{\text{th}} f(z)) \right]. \quad (66)$$

Let $\mathcal{N}_b(> \mathcal{L}_\nu) = N_{b,\text{total}} \hat{\mathcal{N}}(> \mathcal{L}_\nu)$ so that $\hat{\mathcal{N}}(> \mathcal{L}_{\nu,l}) = 1$ and $\hat{\mathcal{N}}(> \mathcal{L}_{\nu,u}) = 0$; for a powerlaw distribution

$$\hat{\mathcal{N}}(> \mathcal{L}_\nu) = \frac{\mathcal{L}_{\nu,u}^{1-\alpha} - \mathcal{L}_\nu^{1-\alpha}}{\mathcal{L}_{\nu,u}^{1-\alpha} - \mathcal{L}_{\nu,l}^{1-\alpha}}. \quad (67)$$

Measure the flux density relative to some reference value S_0 ; at this value, the threshold value of \mathcal{L}_ν is $\mathcal{L}_{\nu,H}^{\text{th}}(S_0)$, the faintest bursts are visible to some reference redshift $z_l(S_0)$, and the brightest bursts are visible to some higher reference redshift $z_{\text{max}}(S_0)$. Then at any other flux density threshold S ,

$$f(z_l(S)) = \frac{f(z_l(S_0))}{S/S_0} \quad f(z_{\text{max}}(S)) = \frac{f(z_{\text{max}}(S_0))}{S/S_0}; \quad (68)$$

Eqs. (68) can be inverted to find $z_l(S)$ and $z_{\text{max}}(S)$ given $z_l(S_0)$ and $z_{\text{max}}(S_0)$, and these relations could be differentiated with respect to S .

Since we are interested in how the burst rate varies with flux density threshold S , we denote $\Gamma_b(\leq z_{\text{max}}(S))$ simply by $\Gamma_b(\geq S)$. In Euclidean space with a z independent star formation rate, $dG_b(z)/dz = z^2$ and $f(z) = z^2$, and $\Gamma_b(\geq S) \propto S^{-3/2}$ independent of the distribution of intrinsic brightnesses, as is well known. depends on a number of parameters, even after fixing cosmological parameters and the star formation rate: $z_l(S_0)$, $z_{\text{max}}(S_0)$, z_c , and α . There are basic trends associated with these parameters:

- High α with low $z_l(S)$ implies $\Gamma_b(\geq S)$ is dominated by intrinsically faint bursts which, in turn, implies that $S^{3/2}\Gamma_b(\geq S)$ remains nearly constant for a wide range of S even when $z_{\text{max}}(S)$ is large.
- For low α , $\Gamma_b(\geq S)$ is dominated by bursts that are both intrinsically bright and have the largest flux densities, so $S^{3/2}\Gamma_b(\geq S)$ drops substantially at low S for $z_{\text{max}}(S) \gtrsim 1$.
- Deviations from constant $S^{3/2}\Gamma_b(\geq S)$ arise as a consequence of curved spacetime geometry, variable star formation rate, and color corrections. The salient effects include:

- (i) $\tilde{r}(z)$ asymptotes at large z , for example, $\tilde{r} \rightarrow 2.28$ in Λ CDM with $\Omega_M = 0.27$;
- (ii) a peak star formation rate at $z \approx 1.86$;
- (iii) slow (approximately logarithmic) increase of $z_{\text{max}}(S)$ at small S for $z_c \approx 1$ as color corrections become significant.

At $z < 1.86$, the rising star formation can cause $S^{3/2}\Gamma_b(\geq S)$ to grow.

The upper panel in Fig. 4 shows a sample of results for $\Gamma_b(\geq S)/\Gamma_b(\geq S_0)$ assuming power law distributions of intrinsic burst brightnesses. We regard $\Gamma_b(\geq S_0)$ as known observationally (e.g. $\sim 10^{3-4}$ per day at $S_0 \simeq 1$ Jy). To aid in interpreting the results, the lower panel shows the mean redshift of outbursts

$$z_{\text{mean}}(S) \equiv \frac{1}{\Gamma_b(S)} \int_0^{z_{\text{max}}(S)} dz z \frac{d\Gamma_b(z, S)}{dz}. \quad (69)$$

We fix $z_l(S_0) = 0.01$, which means that the intrinsically faintest ERBs would only be detectable to a

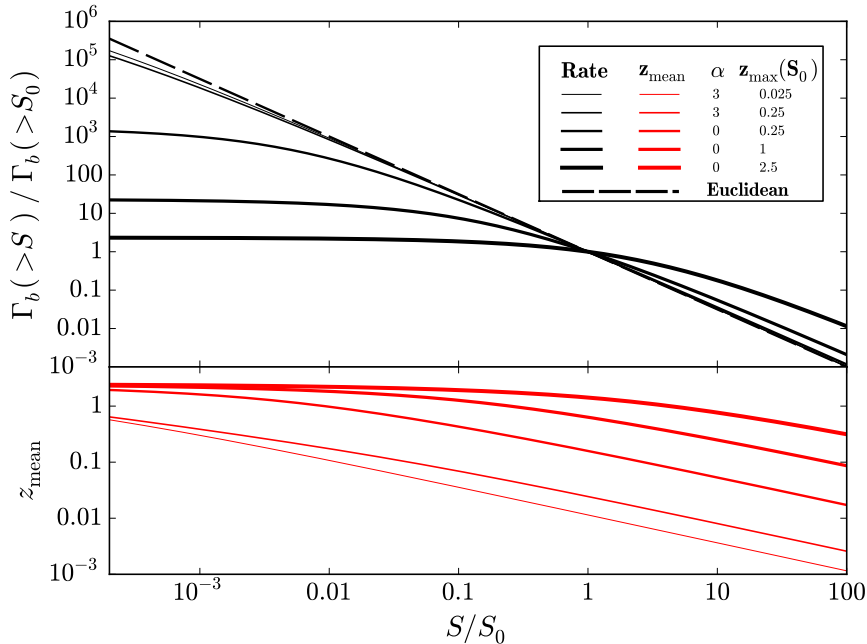


Figure 4. Plot of the scaled burst rate and mean redshift z_{mean} for five combinations of z_{max} and slope α of a power-law luminosity function for individual sources. The rate is normalized to a value of unity at $S/S_0 = 1$. The assumed spectrum has an exponential cutoff $z_c = 1$. The dashed line shows the $(S/S_0)^{-3/2}$ relation for a population of standard candles in Euclidean space. For more details see text (§6.3.2)

distance $\simeq 40$ Mpc at the reference flux density S_0 ; we deliberately chose $z_l(S_0)$ to be large enough that bursts from the Local Group only would occur rarely. We adopt $z_c = 1$ since the most favorable condition for detection is for frequencies near but below the curvature radiation peak. The dashed curve is the Euclidean result $(S_0/S)^{3/2}$, which is shown for comparison. Results are shown for $\alpha = 3$, a *steep* distribution for which the observed bursts are primarily the *intrinsically faintest*, and $\alpha = 0$, a *flat* distribution for which the observed bursts are primarily the *intrinsically brightest*. For $\alpha = 3$ we show results for $z_{\text{max}}(S_0) = 0.025$, for which the intrinsically brightest bursts are only visible to a distance $\simeq 100$ Mpc at the reference flux density threshold S_0 , and $z_{\text{max}}(S_0) = 0.25$, for which the intrinsically brightest bursts are visible to a distance $\simeq 1$ Gpc at S_0 . As can be seen from the figure, deviations from Euclidean are minor even at $S/S_0 \lesssim 10^{-3}$. The lower panel shows that $z_{\text{mean}}(S) \lesssim$ a few tenths at all S/S_0 shown, even though $z_{\text{max}}(S)$ (which is not shown) is quite large ($\simeq 10$ for the lowest S/S_0). The results are dramatically different for $\alpha = 0$, where observations are dominated by the *intrinsically brightest* bursts. To highlight cosmological effects, we show results for $z_{\text{max}}(S_0) = 0.25, 1$ and 2.5 . In all of these cases, $\Gamma_b(S)$ levels off at small S/S_0 ; for $z_{\text{max}}(S_0) = 2.5$ the distribution is even substantially flatter than Euclidean at large flux densities, $S_0 < S < 100S_0$. The lower panel shows that the rate cuts off when $z_{\text{mean}}(S) \gtrsim 1$. However, although $z_{\text{max}}(S) \simeq 10$ for the lowest values of S/S_0 shown, $z_{\text{mean}}(S)$ does not grow rapidly at small S/S_0 , primarily because of the effects of the color correction and diminishing star formation rate.

Leveling off of $\Gamma_b(S)$ at small values of S is a distinctive signature of a cosmological population of ERBs. However, if, in particular, α is fairly large, discerning deviations from the Euclidean distribution would require large and deep samples of bursts. This is because, for a steeply decreasing distribution of intrinsic brightnesses, observations at a given flux density threshold are dominated by sources at relatively low redshifts, where deviations from Euclidean geometry are smallest. Moreover, if the ERBs *already detected* are at typical redshifts $\simeq 1$, the rate of detection at smaller flux density thresholds will only grow by a modest factor: for $\alpha = 0$ and $z_{\text{max}}(S_0) = 2.5$. Fig. 4 shows that $\Gamma_b(S)/\Gamma_b(S_0) \lesssim 2$ for $S/S_0 \geq 10^{-3}$.

Conversely, if the ERBs already detected are primarily “local,” at distances $\lesssim 100 \text{ Mpc} - 1 \text{ Gpc}$, then $\Gamma_b(S)$ continues to rise rapidly with decreasing S/S_0 until cosmological effects intervene.

6.3.3 Role of Gravitational Lensing

The above estimates ignore gravitational lensing, which has been considered by Zheng et al. (2014). Here we consider gravitational lensing by stars; the characteristic Einstein radius for source and lens at $z \sim 1$ is $R_E = \sqrt{4GM/cH_0} \approx 8.9 \times 10^{16} \text{ cm} (M/M_\odot)^{1/2}$, much larger than stellar radii. Amplifications are $A(b) \sim R_E/b$ for rays passing at impact parameter $b \ll R_E$, and the maximum amplification is $A(R) \sim 1.3 \times 10^6 (M/M_\odot)^{1/2} (R_\odot/R)$. The duration of a lensing event with amplification A is $R_E/Av \sim 94A^{-1} (M/M_\odot)^{1/2} (v/300 \text{ km s}^{-1})^{-1}$ years, where v is a characteristic relative speed between lens and source projected onto the sky. Because we are interested in short-lived pulses, it is the lensing probability that is relevant, not the lensing rate, which is appropriate for steady light sources, such as the stars monitored in microlensing surveys. The probability density for A is $p(A)dA \sim \Omega_\star A^{-3} dA$ at large A ,

$$P(A) = Ap(A) \sim \frac{\Omega_\star}{A^2} \approx \frac{0.003\Omega_{\star,0.003}}{A^2} \quad (70)$$

is a measure of the probability of lensing amplification $\sim A$ out to $z \sim 1$. Thus, the rate of bursts that are visible because of amplification by gravitational lensing is

$$P(A)\Gamma_{b,H} \sim \frac{0.003\Omega_{\star,0.003}\Gamma_{b,H}}{A^2} = \frac{0.003\Omega_{\star,0.003}\Gamma_{b,\text{obs}}}{A^2} \left(\frac{d_H}{d_{\text{max}}} \right)^3, \quad (71)$$

assuming that *unlensed* bursts detectable only out to distance d_{max} can account for the observed rate by themselves. The amplification factor needed to render a burst at $z \sim 1$ detectable is $\simeq (d_H/d_{\text{max}})^2$, assuming that the intrinsic burst brightness is the same as those detected without lensing, so the fraction of bursts that are detectable from $z \sim 1$ as a result of lensing is

$$f_{\text{lens}} \sim \frac{0.003\Omega_{\star,0.003}}{(d_H/d_{\text{max}})} \quad (72)$$

which is $\sim 10^{-4}$ for $d_{\text{max}} = 100 \text{ Mpc}$. Nevertheless, lensed ERBs from $z \sim 1$ may be observable of order once per day.

6.4 DM Contributions from Galaxy Clusters

As stated earlier, ERB host galaxies can provide a significant fraction of the burst’s DM and therefore play a strong role in establishing the ERB distance scale. Here we discuss the contribution to DMs from galaxy clusters, either as sites for host galaxies or as intervening structures.

Following Arnaud et al. (2010), we parameterize the electron column density in a cluster via the mass M_η of a region within which the mean density is η times the closure density at the redshift of the cluster (see also Nagai et al. (2007) and Voit (2005)). In this prescription, $R_\eta = [2GM_\eta/\eta H^2(z)]^{1/3}$ and we estimate the electron column density to be

$$DM_\eta \approx \frac{3f_{\text{bary}}\eta H^2(z)R_\eta(1+X)}{16\pi Gm_p} \approx 340h_{0.7}^{4/3} \text{ pc cm}^{-3} \left(\frac{M_\eta}{10^{14}M_\odot} \right)^{1/3} \left(\frac{\eta}{500} \right)^{2/3} \left(\frac{f_{\text{bary}}}{0.2} \right) \left(\frac{1+X}{1.75} \right) [E(z)]^{4/3}. \quad (73)$$

where f_{bary} is the baryon density fraction and X is the H fraction by mass in the cluster gas; $\eta = 500$ is commonly used in fitting data on SZ clusters with generalized NFW pressure profiles (e.g. Planck Collaboration et al. (2015)). The characteristic dispersion measure implied by Eq. (73) is substantial, and given that the electron density varies significantly within a cluster, DM values several times larger or

smaller than Eq. (73) may be encountered for different lines of sight. Since the escape velocity is

$$\sqrt{\frac{GM_\eta}{R_\eta}} \approx 780 h_{0.7}^{2/3} \text{ km s}^{-1} \left(\frac{M_\eta}{10^{14} M_\odot} \right)^{1/3} \left(\frac{\eta}{500} \right)^{1/6} [E(z)]^{1/3}, \quad (74)$$

neutron stars are unlikely to escape the galaxy cluster even if they are able to escape the galaxies where they were born; moreover, $1 \text{ Mpc}/1000 \text{ km s}^{-1} = 0.98 \text{ Gyr}$, so even a fast-moving neutron star is unlikely to cross a cluster during its lifetime as a pulsar, much less during its first ~ 1000 active years. Using the $M_{500} - Y_{500}$ relationship from Eq. (5) in Planck Collaboration et al. (2014) (see also Eqs. (25)-(27) in Arnaud et al. (2010)) we find a $\text{DM}_{500} - Y_{500}$ relationship:

$$\text{DM}_{500} \approx 740 h_{0.7}^{0.50} \text{ pc cm}^{-3} \left(\frac{Y_{500}}{10^{-4} \text{ arcmin}^2} \right)^{0.19} \frac{[E(z)]^{1.2}}{1+z} \left[\frac{\tilde{r}(z)}{1+z} \right]^{0.37}. \quad (75)$$

(The additional factor of $1+z$ arises from the redshift of the radiation frequency between the cluster and observer.) Using the approximate mass (M_{500})-richness (N_{200}) relationship from Rozo et al. (2014), we find a DM -richness relationship (see also Bauer et al. (2012))

$$\text{DM}_{500} \approx 440 \text{ pc cm}^{-3} (N_{200}/40)^{0.35 \pm 0.04}. \quad (76)$$

The relationships underlying Eq. (76) were derived for clusters at modest redshifts ($z \lesssim 0.3$; Rozo et al. (2009)), so we have not included detailed z dependences in Eq. (76).

McQuinn (2014) has demonstrated that a large ERB sample can be used to probe the distribution of “missing” baryons in the universe by analyzing DM values as a function of proximity of lines of sight to galaxy clusters. In the next section we consider the likelihood of such proximities and the role of clusters in establishing a distance scale for ERBs.

7 SUMMARY OF CONSTRAINTS ON ERB POPULATIONS

Here we consolidate constraints on ERB source distances made in previous sections on the basis of NS population numbers and radiation physics in NS magnetospheres. We also incorporate the likely contributions to ERB dispersion measures from galaxy clusters for at least some of the ERBs.

Figure 5 shows constraints on N_b , the number of bursts per NS (black lines), and on N_i , the number of shot pulses per burst needed to account for measured flux densities (blue line), as a function of maximum population distance. The two lines for N_b correspond to full-sky burst rates of 10^3 and 10^4 d^{-1} and indicate that only a small number is needed per NS if the detectable population extends to $\sim 1 \text{ Gpc}$. For smaller d_{max} , repeats may be expected if the burst phase of a given NS is short, such as the current phase of the Crab pulsar (1000 yr) but are not expected if ERBs occur predominantly from older, possibly dormant NS, that are $> \text{Gyr}$ in age. The number of shots per ERB increases rapidly with d_{max} and is based on assuming that individual shots are limited by radiation reaction and particle number densities expected in NS magnetospheres. The shaded region on the right indicates that energy requirements become increasingly severe as d_{max} increases from a few hundred Mpc to larger distances. The shaded region on the left represents the approximate 80 Mpc radius of the local Laniakea supercluster (Tully et al. 2014), comprising at least 10^5 galaxies distributed in prominent galaxy clusters, including the Virgo cluster. The corresponding galaxy density $\sim 2 \text{ deg}^{-2}$, so the lack of associations of detected ERBs with any galaxies in the local supercluster suggests $d_{\text{max}} \gtrsim 80 \text{ Mpc}$.

The unshaded region in the figure between 80 and 300 Mpc constitutes a plausible but by no means required range for d_{max} . The distances in this range are near enough that cosmological effects are minimal, but far enough that it is unlikely that repeat bursts would be detected from any particular NS.

Additional constraints on the ERB distance scale involve the possible contributions of galaxy clusters

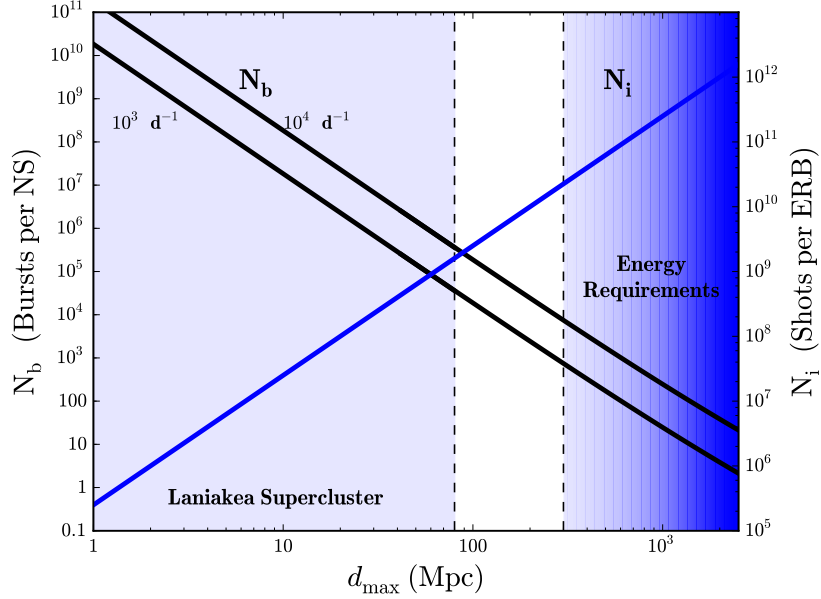


Figure 5. Plot showing the number of bursts per NS (N_b) and the number of shot pulses per ERB (N_i) needed to account for the apparent total sky rate of ERBs and their flux densities. Two curves are shown for N_b based on ERB rates of 10^3 and 10^4 d^{-1} . The shaded region on the left indicates the approximate size of the Laniakea supercluster (Tully et al. 2014), which is approximately the distance out to which there is about one L^* galaxy per deg^2 . On the right, the increasingly darker shading indicates that ERBs challenge the energy requirements of coherent radiation.

to DMs. As shown previously, cluster DMs are large enough to account for much of the DM in excess of the contribution from the Milky Way's ionized gas. However, we need to consider the likelihood for an ERB source either residing within or being viewed through a cluster. For an overdensity η , a cluster's angular size corresponding to R_η at redshift z is

$$\begin{aligned} \theta_\eta &= \left(\frac{2GM_\eta H_0}{\eta c^3} \right)^{1/3} \frac{1+z}{[E(z)]^{2/3} \tilde{r}(z)} = \frac{0.57 \text{ arcmin} (1+z)}{(\eta/500)^{1/3} [E(z)]^{2/3} \tilde{r}(z)} \left(\frac{M_\eta h_{0.7}}{10^{14} M_\odot} \right)^{1/3} \\ &\approx \frac{2.4 \text{ arcmin}}{(\eta/500)^{1/3} h_{0.7}^{2/3} d_{\text{Gpc}}} \left(\frac{M_\eta}{10^{14} h_{0.7}^2 M_\odot} \right)^{1/3} \end{aligned} \quad (77)$$

where we used the low redshift approximation $\tilde{r}(z)[E(z)]^{2/3}/(1+z) \simeq z \simeq H_0 d/c \approx 0.23 h_{0.7} d_{\text{Gpc}}$ in the last line of Eq. (77). The expected number of cluster intersections made by a line of sight is

$$N_{\text{C,int}} = \pi n_{\text{C},0} \int dz \theta_\eta^2(z) \frac{dr_c(z)}{dz} r_c^2(z) \quad (78)$$

where $n_{\text{C},0} = 3f_C \Omega_m H_0^2 / 8\pi G M_C$ is the comoving density of clusters assuming that a fraction f_C of the mass of the Universe is in clusters of mass M_C ; below, we take $M_C = M_\eta$ and $\eta = 500$ for numerical estimates. Using Eq. (77) we find

$$\begin{aligned} N_{\text{C,int}} &= \frac{3f_C \Omega_m c}{4(2GM_\eta H_0 \eta^2)^{1/3}} \int_0^z \frac{dz' (1+z')^2}{[E(z')]^{7/3}} \approx \frac{0.27(f_C/0.1)(\Omega_m/0.3)}{(M_{500} h_{0.7}/10^{14} M_\odot)^{1/3} (\eta/500)^{2/3}} \times \frac{2}{\Omega_m} \left\{ 1 - \frac{1}{[E(z)]^{1/3}} \right\} \\ &\approx \frac{0.06 d_{\text{Gpc}} h_{0.7}^{2/3} (f_C/0.1)(\Omega_m/0.3)}{(M_{500}/10^{14} M_\odot)^{1/3} (\eta/500)^{2/3}}, \end{aligned} \quad (79)$$

where the second line is for low z ; for a distribution of masses, we replace $M_{500}^{-1/3}$ by its mean, which may

be skewed toward lower masses, depending on the galaxy cluster mass distribution. According to Eq. (79), intersections are rather likely (30%) out to $z \simeq 1$, and approaches $\simeq 1$ at larger z . Moreover, intersections are likelier at smaller density contrasts: $N_{C,\text{int}} \propto M_\eta^{-1/3} \eta^{-2/3}$, and M_η ultimately levels off as η decreases.

The expected angular separation θ_1 between a given line of sight and the nearest cluster is

$$\theta_1 = \left[\frac{8GM_C H_0}{f_C \Omega_m c^3 \tilde{r}^3(z)} \right]^{1/2} \approx \frac{1.9 \text{ arcmin} (M_C h_{0.7}/10^{14} M_\odot)^{1/2}}{(f_C/0.1)^{1/2} (\Omega_c/0.3)^{1/2} [\tilde{r}(z)]^{3/2}} \approx \frac{17 \text{ arcmin} (M_C/10^{14} M_\odot)^{1/2}}{(f_C/0.1)^{1/2} (\Omega_c/0.3)^{1/2} h_{0.7} d_{\text{Gpc}}^{3/2}}, \quad (80)$$

where once again the last approximation is for low z , where $\tilde{r}(z) \simeq z \simeq H_0 d/c$. Therefore, the probability that the line of sight to a particular FRB passes close to a cluster is fairly large if FRBs may be seen out to $d_{\text{Gpc}} \simeq 1$. This estimate ignores clustering of clusters, which enhances the probability of seeing additional clusters near the direction to a particular cluster.

Various studies of the galaxy cluster mass function are consistent with $f_C \sim 0.05 - 0.1$, with a cut-off above $M_\star \sim 10^{14} M_\odot$. (e.g Bahcall 1996, 1999; Reiprich & Böhringer 2002; Rines et al. 2007; Wen et al. 2010; Tempel et al. 2014). The probability that an ERB originates either within or behind a cluster is therefore $\sim 10 - 15\%$ if $d_{\text{Gpc}} \simeq 1$; the probability is $\sim 35 - 40\%$ for ERBs originating from $z \gtrsim 1$. These probabilities are high enough that some of the ERBs detected to date may have been located in or behind clusters of galaxies; the DMs for such an ERB will have a considerable contribution from the cluster. Thus, FRB redshifts and distances inferred under the assumption that DMs arise solely from a smooth IGM are overestimates: actual redshifts and distances are likely to be smaller.

Because of the DM fluctuations introduced by clusters and their environs, it is not unlikely that two FRBs separated by ~ 10 arcmin on the sky have DMs that differ by $\sim 300 \text{ cm}^{-3} \text{ pc}$ (see McQuinn 2014, and Eqs. (73) and (80)). This may be the explanation for why FRBs 110220 and 140514, which are separated by about 9 arcmin on the sky, have DMs that differ by about 380 pc cm^{-3} ; see Thornton et al. (2013) and Petroff et al. (2015c). Although we do not offer any scenario in which it is likely that two FRBs are that close on the sky, given that they are, the line of sight to FRB 110220 may pass through a cluster, whereas the line of sight to FRB 140514 passes outside. This unlikely coincidence of positions on the sky may therefore offer indirect evidence for the extragalactic origin of these FRBs, since the additional contribution from an intervening galaxy cluster accounts simply for their DM difference.

8 OBSERVATIONAL TESTS

We expect a number of observational features from an ERB source population comprising extragalactic NS, some of which constitute tests of the model. Some of these features in fact are generic to *any* extragalactic source population.

8.1 Temporal Substructure, Polarization, and Faraday Rotation of ERBs

ERB pulses with ms durations are necessarily composed of sub-ns shot pulses, regardless of the nature of the emitting source. Our analysis of the NS-magnetosphere case suggests that the number of shot pulses must be very large, indicating that ERBs analyzed with high time resolution will be consistent with amplitude-modulated noise. However, a nearby (low- z) population requires far fewer shot pulses, raising the prospect that individual shot pulses or other substructure might be detectable. However, pulse broadening from extragalactic scattering will prevent detection of shot pulses for at least some of the objects where scattering is seen. Detection of individual shot pulses would imply that the underlying population of ERB sources is nearby on a cosmological scale and would require that scattering broadening of pulses generally be small.

While we expect a null result, it nonetheless is worthwhile to use radio telescope backend processors with sub- μs resolution and test whether the shot noise has a very high rate, as we conclude, or a low

rate. Polarization measurements may be informative about magnetic field conditions in ERB sources and whether depolarization occurs from incoherent summing of shot pulses and from propagation effects in the sources or along the line of sight.

ERB polarization also may indicate whether the ms-pulse duration is associated with rotation of a beam, as in radio pulsars, or due to true temporal modulation, which might yield a constant polarization state. Single pulses from pulsars generally show elliptical polarization and a rotation of the plane of polarization across the pulse, which is consistent with relativistic beaming from particles moving along curved magnetic field lines combined with the pulsar’s spin. However, individual shot pulses from the Crab pulsar show large degrees of circular polarization and changes in handedness between neighboring shot pulses that are argued to be due to temporal modulations (Hankins et al. 2003). Linearly polarized ERBs can be used to measure Faraday rotation along the line of sight. If ERB sources are embedded in host galaxies, a wide range of rotation measures $|\text{RM}| \leq 500 \text{ rad m}^{-2}$ can be expected (Oppermann et al. 2012). Contributions to RM from intergalactic gas have been identified (Xu et al. 2006; Kronberg et al. 2008) that would be relevant to ERB sources outside spiral galaxies at high redshifts.

8.2 Reobservations and Localization of ERB Lines of Sight

Attempts to redetect ERBs from a particular object are problematic for any large source population, such as extragalactic NS. In Section 6.1 we demonstrated that reobservations do not provide definitive constraints on the event rate per NS if the population extends to cosmological distances because many NS are within the instantaneous FoV of the largest single-dish telescopes and, for distant populations, even within the synthesized beam of array telescopes. For example, observations with the VLA in its A configuration at 1.5 GHz provide a synthesized beam width ~ 1 arc sec that includes $\sim 2000 d_{\text{Gpc}}^3$ NS. So long as ERBs from a given source are not bunched in time, it is equally likely for any of these sources to emit a burst after an initial one is discovered. One source per FoV requires either a VLB array with milli-arcsec resolution or a population with $d_{\text{max}} \lesssim 80$ Mpc. While the dispersion measure can be used to discriminate between sources, if it is dominated by the intergalactic medium the many sources at similar redshifts will show similar values.

Localization of ERB sources would allow discrimination between a young NS population, which is expected to be associated with star-forming galaxies, and old objects which may have no association if they involve sources kicked out of galaxies. However, sources are not likely to be disassociated from galaxy clusters, so larger ERB samples can be tested for coincidence with cluster catalogs as well as galaxy catalogs. Any galaxy-ERB associations combined with redetections in followup observations would allow one to argue statistically that the original ERB source has been redetected even if there are many NS within the telescope FoV.

8.3 Interstellar Scintillation and Extragalactic Scattering

Diffraction interstellar scintillations (DISS) are seen from Galactic pulsars as a consequence of multi-path propagation. Fully-modulated (100%) intensity variations in time and frequency require a source size smaller than the isoplanatic angle, $\theta_{\text{iso}} \approx \lambda/D\theta_{\text{s,ISM}}$, where $\theta_{\text{s,ISM}}$ is the scattering diameter (e.g. Cordes & McLaughlin 2003). Larger sources will attenuate DISS by a factor $\theta_{\text{psr}}/\theta_{\text{iso}}$. For kpc distances and mas scattering angles, $\theta_{\text{iso}} \approx 0.4 \mu\text{as } \nu^{1.2} D_{\text{kpc}}^{-1}$. For lines of sight at high Galactic latitudes, the distance D is replaced by the scale height $H_{\text{ISM}} \approx 0.5$ kpc. The NE2001 model (Cordes & Lazio 2002) uses a distributed model for the scattering and yields $\theta_{\text{iso}} \approx 2 \mu\text{as } \nu^{1.2}$ at a Galactic latitude $b = 90^\circ$.

Magnetospheres of Galactic pulsars easily satisfy $\theta_{\text{psr}} \lesssim \theta_{\text{iso}}$. Galactic pulsars have measured characteristic time scales of seconds to hours and characteristic bandwidths of tens of kHz to 100 MHz. ERB sources should show DISS if they are intrinsically small, as they must be from light-travel arguments,

but only if they are not angularly broadened significantly by scattering along the extragalactic portions of their lines of sight. We therefore consider extragalactic scattering in either the IGM, a host galaxy, or a galaxy cluster combined with scattering in the foreground ISM. Temporal scintillations of ERBs cannot be measured in any case because the burst duration is short. However, frequency structure in the spectrum is potentially measurable.

Several ERBs show pulse asymmetries with the strong frequency dependence indicative of plasma scattering. Given their high Galactic latitudes, this scattering must be due to extragalactic scattering. We use the scattering time τ_s to estimate the scattering diameter and compare it to the isoplanatic angle for DISS. For a thin scattering screen at distance D_s from the source, the pulse broadening time is $\tau_s = g_s D \theta_o^2 / 2c$, where θ_o is the scattered source size and $g_s = D/D_s - 1$ takes into account the scattering geometry. ERB scattering times ~ 1 ms imply $\theta_o \approx \sqrt{2c\tau_s/g_s D} \approx 30 \mu\text{as} \sqrt{\tau_{\text{ms}}/g_s D_{\text{Gpc}}}$.

First consider scattering midway along the LOS, $D_s = D/2$, which gives $g_s = 1$. The scattering diameter ‘seen’ by the foreground ISM is then too large to show DISS, particularly for sources nearer than 1 Gpc. No frequency structure is expected in the spectrum for this reason and also because its characteristic bandwidth would be $\Delta\nu_{\text{DISS}} \approx 1/2\pi\tau_s \approx 160$ Hz.

However, extragalactic scattering close to the source with $D_s \ll D$ yields $g_s \gg 1$ and a much smaller scattered source diameter. For $D_s \sim 1$ Mpc, as might be appropriate for a source scattered by ionized gas in an ERB’s host cluster, $\theta_o \approx 0.9 \mu\text{as} \sqrt{\tau_{\text{ms}} D_{\text{s,Mpc}}/D_{\text{Gpc}}}$ which is small enough to allow fully-modulated DISS. Sources embedded in and scattered by a host galaxy with $D_s \sim 1$ kpc imply even smaller source sizes (by a factor of 30).

When diffractive interstellar scintillations are expected, the frequency structure will have a characteristic scale given by $\Delta\nu_{\text{DISS}} \sim 1/2\pi\tau_{\text{s,ISM}}$ where $\tau_{\text{s,ISM}}$ is the pulse broadening time expected from scattering in the Milky Way. For $b = 90^\circ$, a scintillation bandwidth $\Delta\nu_{\text{DISS}} \sim 4$ MHz is expected. Scintillation structure on frequency scales of this order can be searched for and would demonstrate that extragalactic scattering occurs close to the source. Absence of frequency structure of course would imply that scattering is more distributed along the line of sight.

8.4 Giant Pulse Energetics

Much of our discussion has involved the energetics of radio bursts that refer to previously observed giant pulses from the Crab pulsar. It would be highly informative to monitor the Crab pulsar over thousands of hours, much longer than the longest dwell times to date, in order to identify or constrain a maximum in the distribution of pulse amplitudes. Any such maximum for the Crab pulsar may signify similar maxima in the distributions of ERB amplitudes from particular sources and from the ensemble of sources.

9 SUMMARY & CONCLUSIONS

In this paper we have examined the hypothesis that fast radio bursts are associated with rare, bright pulses from extragalactic neutron stars. Our motivation is twofold. First, NS are known to emit bright pulses with a wide range of durations, including the ms widths of ERBs, so associating fast radio bursts with extragalactic NSs involves extrapolation from known phenomena. Second, the large number of NS that exist in a Hubble volume can easily produce the inferred ERB rate even if only a single burst is produced in the lifetime of each NS. An added virtue, however, is that multiple bursts per object allow the population to be closer and relax the energy requirements on the radiation process. The multiplicity can still be small enough that no individual source would repeat over time scales of months to even centuries. However, the source population could be near enough for repeats to be observed on human time scales. By contrast, burst interpretations involving one-off events per object, such as evaporating black holes or from stellar implosions, necessarily require a large cosmological volume to account for the ERB rate. Finally, even if

NS do not turn out to be the source population, we consider it a matter of due diligence to consider NS prior to invoking more exotic explanations.

We have found that the radiation mechanism is highly constrained. Independent of the source population, sub-ns structure in the radiation field must be produced through a coherent process and the overall ms widths of ERBs require incoherent superposition of a large number of individually coherent shot pulses. We have specifically examined curvature radiation in conditions similar to the magnetospheres of active pulsars. Such radiation can account for the lone, 2 MJy shot pulse from the Crab pulsar measured by Hankins & Eilek (2007) via coherent radiation from a nearly neutral clump, with net charge $\sim 10^{21}e$ and total lepton number $\gtrsim 10^{27}$, near the light cylinder. The radiation strength of the Crab shot pulse, measured as fluence times distance squared, $\sim 1 \text{ MJy-ns-kpc}^2 = 1 \text{ Jy-ms-kpc}^2$. ERBs have strengths $\sim 10^{12} d_{\text{Gpc}}^2 \text{ Jy-ms-Gpc}^2$. Such large radiation strengths cannot be due to single coherent regions because the ms time scales require a temporal spread of shot-pulse arrival times. If an ERB comprises numerous shot pulses that individually are of order the largest seen from the Crab pulsar, the number involved is $\sim 10^{12} d_{\text{Gpc}}^2$, which is sensitive to distance but very large at all extragalactic distances. However, we note that large numbers of shot pulses comprise single pulses from most pulsars, which have durations up to 100s of ms. Comparing the total energy available to fuel an outburst from a NS magnetosphere to the total energy required observationally yields a maximum source distance; for an outburst originating near the light cylinder of a Crab-like NS ($P \approx 30 \text{ ms}$, $\dot{P}/P \approx (1000 \text{ years})^{-1}$) we find $d_{\text{Gpc}} \lesssim 0.1$. Bursts from ordinary pulsars are similarly constrained to arise from local group galaxies but in some circumstances (namely large magnetic fields and low emission altitudes) could be seen from further away. Bursts from magnetars could similarly originate from the local group and perhaps further. These rough distance bounds can be extended to $d_{\text{Gpc}} \simeq 1$ if outbursts underlying ERBs are associated with young NS (large \dot{P}/P and small P), especially if the outburst occurs well within the light cylinder, where the magnetic field and available magnetospheric energy reservoir are larger. However, there may be a lower bound on the emission altitude $\sim cW_i$ based on measured ERB widths $W_i \sim \text{ms}$, and the time needed for coherence to be established.

A triggering mechanism is needed for infrequent, high amplitude bursts from NS (or from any source that repeats). For emission from a magnetosphere, the trigger could either be internal, such as from an extraordinarily large rotation-altering event (e.g. a spin glitch), or external, such as infalling debris (e.g. Cordes & Shannon 2008) that stimulates a pair cascade or from a large reconnection event in NS magnetotails that injects particles and energy into the magnetosphere. Internal triggers may inject more energy than can be carried in by external material or charges. However, external triggers may indicate an important role for the local environment of ERB sources. Environmental effects, in turn, have implications for the relative contributions to ERB dispersion measures.

DMs of ERBs have largely been attributed to the IGM combined with a foreground contribution from the Milky Way and a similar amount from the host galaxy⁷, yielding relatively high redshifts derived from the required, substantial IGM contribution. Generally, an intervening galaxy or host or intervening galaxy cluster will also make contributions, as will any dense gas local to the source itself. We note that the relatively large redshifts attributed to ERBs ($0.5 \lesssim z \lesssim 1$) yield a non-negligible probability for the line of sight encountering a galaxy cluster; additionally, some ERB sources may reside within clusters. Since clusters can account for a large fraction of the measured DMs, ignoring them is inconsistent with the attributed redshifts for at least some of the ERBs. If the local environment plays a role in triggering ERBs, the underlying sources may reside in dense regions within host galaxies, therefore providing another sizable contribution to DMs. An extreme case would be triggering by jet particles from supermassive black

⁷ We note that a few authors have argued that ERBs are in fact Galactic sources.

holes in galactic centres, which could account for most of the measured DMs and allow the population to reside at small d_{\max} .

As others have stated (e.g. Law et al. 2015), the most valuable new observations will be the localization of ERB sources through high time resolution radio imaging. These will allow a determination of the distance scale and provide constraints on the contributions of host galaxies and the IGM to dispersion measures. Our analysis suggests that it is unlikely that X-and- γ -ray emission will be seen from ERBs if the ratio of high energy emission to radio emission scales like that from pulsars.

We thank Shami Chatterjee and Tim Hankins for useful conversations and Jean Eilek and Tim Hankins for providing the data used in Figure 1. We also thank the anonymous referee for several suggestions that improved the paper significantly. This work was supported by NSF Grant Phys 1104617 and NASA grant NNX13AH42G.

APPENDIX A: SHOT NOISE WITH VARIABLE RATE AND AMPLITUDE

Consider a (scalar) shot pulse $E(t)$ with duration $W_s \lesssim 1$ ns whose Fourier transform $\tilde{E}(\nu) = \int dt E(t)e^{-2\pi i\nu t}$ is sampled with a receiver with bandwidth $\Delta\nu_r$ centred on a frequency ν_0 . The selected electric field for a rectangular bandpass shape is

$$E(t, \nu_0; \Delta\nu_r) = \int_{\nu_0 - \Delta\nu_r/2}^{\nu_0 + \Delta\nu_r/2} d\nu \tilde{E}(\nu) e^{+2\pi i\nu t} + \text{CC}, \quad (\text{A1})$$

where the negative frequencies correspond to the complex conjugate of the first term. For an unresolved pulse with an intrinsic bandwidth $\sim W_s^{-1} \gg \Delta\nu_r$, we have

$$E(t, \nu_0; \Delta\nu_r) \approx \Delta\nu_r \tilde{E}(\nu_0) e^{+2\pi i\nu_0 t} \text{sinc } \Delta\nu_r t + \text{CC}, \quad (\text{A2})$$

where $\text{sinc } x = (\sin \pi x)/\pi x$. This equation will be approximately valid even for $W_s^{-1} \gtrsim \Delta\nu_r$. In practice, the signal is usually heterodyned to zero frequency (baseband) through multiplication by $e^{-2\pi i\nu_0 t}$ to obtain the complex pulse $\Delta\nu_r \tilde{E}(\nu_0) \text{sinc } \Delta\nu_r t$. Dispersion in ionized gas is not included in the model because it is assumed to be removed as one of the operations made on the baseband signal. Scattering is also excluded here though it will cause individual shots to overlap and is a factor in the assessment of total ERB widths.

The power collected in a unit area is $\sim (c/2\pi)|E(t, \nu; \Delta\nu_r)|^2$ so the measured flux density of a single shot is

$$s_{\nu_0}(t) = \frac{c\Delta\nu_r |\tilde{E}(\nu_0)|^2 \text{sinc}^2 \Delta\nu_r t}{2\pi} \equiv s_{\nu_0, \text{max}} \text{sinc}^2 \Delta\nu_r t. \quad (\text{A3})$$

The measured shot pulse and its maximum $s_{\nu_0, \text{max}}$ both depend on the receiver bandwidth but the fluence A_{ν_0} (the integrated flux density) is independent of the bandwidth because $\Delta\nu_r \int dt \text{sinc}^2 \Delta\nu_r t = 1$,

$$A_{\nu_0} = \int dt s_{\nu_0}(t) = \frac{s_{\nu_0, \text{max}}}{\Delta\nu_r} = \frac{c|\tilde{E}(\nu_0)|^2}{2\pi}. \quad (\text{A4})$$

An incoherent superposition of coherent shot pulses accounts for the electromagnetic and statistical properties of observed pulses with ms durations, as described in the main text. Superposing shot pulses like Eq. A2, each having width $\sim \Delta\nu_r^{-1}$, arrival time t_{s_j} , and amplitude $\Delta\nu_r \tilde{E}_j(\nu)$, the electric field is

$$E(t, \nu, \Delta\nu_r) = \Delta\nu_r \sum_j \tilde{E}_j(\nu) e^{2\pi i\nu(t-t_{s_j})} \text{sinc } \Delta\nu_r(t-t_{s_j}), \quad (\text{A5})$$

where we have dropped the subscript on the center frequency.

When the number of shots is large, the total flux density is the sum of terms like Eq. A3,

$$S_\nu(t) \approx \sum_j s_{\nu, \text{max}_j} \text{sinc}^2 \Delta\nu_r(t-t_{s_j}); \quad (\text{A6})$$

cross terms between shot pulses are negligible because phases associated with the arrival times t_{s_j} are assumed statistically independent. Using the characteristic function of a Poisson process (Rice 1944; Papoulis 1991), the ensemble average depends on the mean of the product of the shot pulse rate $\eta_s(t)$ and the shot amplitude $s_{\nu, \text{max}}(t)$,

$$\langle S_\nu(t) \rangle \approx \int dt' \langle \eta_s(t') s_{\nu, \text{max}}(t') \rangle \text{sinc}^2 \Delta\nu_r(t-t') \approx \langle \eta_s(t) A_\nu(t) \rangle, \quad (\text{A7})$$

where we have defined the fluence per shot, $A_\nu(t) = s_{\nu, \text{max}}(t)/\Delta\nu_r$. The second equality follows because the composite pulse is typically much broader than $\Delta\nu_r^{-1}$, requiring that the rate and mean amplitude vary slowly compared to the sinc^2 function.

Individual pulses have the same form as the ensemble average in Eq. A7 but are noisy from the finite

number of shot pulses. Factoring the rate and fluence for simplicity, the flux density is

$$S_\nu(t) = \eta_s(t)A_\nu(t). \quad (\text{A8})$$

An ERB comprising N_i incoherently summed shot pulses over a width W_i has a mean rate $\eta_s \simeq N_i/W_i$. Alternative forms for the *peak* flux density of the ERB are then

$$S_{\nu,\max} \approx s_{\nu,\max} \left(\frac{\eta_s}{\Delta\nu_r} \right) \approx N_i s_{\nu,\max} \left(\frac{W_r}{W_i} \right), \quad (\text{A9})$$

where the time scale $W_r = 1/\Delta\nu_r$. The first expression says that the peak ERB flux density is larger than the peak single-shot flux density by the ratio of the shot rate to the bandwidth, which can be large. The second says that the ERB peak is equal to the total flux density in all the shots diluted by the factor $W_r/W_i \ll 1$.

The expressions given so far use the ‘native’ resolution of the receiver bandwidth, which will be less than $1 \mu\text{s}$, typically. Data are usually smoothed over many such resolution elements to a time scale τ_{smooth} that is somewhat smaller than the actual pulse width W_i to approximate matched-filtering detection. In this case we would make the replacements $W_r = 1/\Delta\nu_r \rightarrow \tau_{\text{smooth}}$ and $s_{\nu,\max} \rightarrow s_{\nu,\max} \times W_r/\tau_{\text{smooth}}$, leaving the peak ERB flux unchanged in the mean, as expected.

APPENDIX B: CONDITIONS FOR COHERENCE

Let the observer be in direction $\hat{\mathbf{n}}$ relative to the the source, and let $t_{e,c}$ be the time when emission is optimally beamed toward the observer, for a given accelerated charge moving on a path with radius of curvature r_c . This is the time when $\kappa = 1 - \hat{\mathbf{n}} \cdot \mathbf{v}(t_e)$ is smallest; for strong beaming, this happens when $\hat{\mathbf{n}} \cdot \mathbf{a}(t_e) = 0$ (i.e. when the acceleration is perpendicular to the line of sight), which is not guaranteed to occur but is required for super-bright emission. At this time, the charge is at $\mathbf{r}(t_{e,c})$. The electromagnetic field at an observation point (t, \mathbf{r}) depends on $c(t - t_{e,c}) - \hat{\mathbf{n}} \cdot [\mathbf{r} - \mathbf{r}(t_{e,c})]$. For example, for curvature radiation from a charge q moving along an instantaneously circular path with curvature $\hat{\mathbf{c}}r_c$, the electric field for an observer at $\hat{\mathbf{n}}d$ is

$$\frac{dr_c \mathbf{E}(t, \hat{\mathbf{n}}d)}{q} \approx \frac{\hat{\mathbf{c}}(1 - \psi_e^2) + 2\hat{\mathbf{c}} \times \hat{\mathbf{n}} \psi_e \epsilon / \sqrt{2\kappa_0}}{\kappa_0^2 (1 + \psi_e^2)^3} \quad (\text{B1})$$

where $\psi_e = (\sqrt{\psi^2 + 1} + \psi)^{1/3} - (\sqrt{\psi^2 + 1} - \psi)^{1/3}$ with $\psi = (3/2r_c\kappa_0^{3/2})[ct - d - (ct_{e,c} - \hat{\mathbf{n}} \cdot \mathbf{r}(t_{e,c}))]$ and $\kappa_0 = 1 - v \cos \epsilon \simeq \frac{1}{2}(\epsilon^2 + 1/\gamma^2)$. Geometrically, the observer is at angle ϵ above the plane of the (instantaneously circular) orbit of the emitting particle. The electric fields for a collection of particles with a range of peak emission times and positions $\Delta t_{e,c}$ and $\Delta \mathbf{r}(t_{e,c})$ add coherently at frequencies below ω_{coh} if

$$|\Delta[ct_{e,c} - \hat{\mathbf{n}} \cdot \mathbf{r}(t_{e,c})]| \lesssim r_c (2\kappa_{coh})^{3/2} = r_c \left(\epsilon_{coh}^2 + \frac{1}{\gamma^2} \right)^{3/2} \equiv \frac{c}{\omega_{coh}}, \quad (\text{B2})$$

where $|\epsilon| = |\epsilon_{coh}|$ at ω_{coh} .

Eq. (B2) is derived by considering how long a pulse from a given charge is bright as *seen by the observer*. Eq. (B2) has a simple interpretation: at the observer, sharply pulsed electric fields will add up coherently if they overlap. At a given frequency ω in a Fourier decomposition, the observer detects a superposition of electric fields with different phases; the phase associated with reaching optimal beaming at time $t_{e,c}$ is $\omega[ct_{e,c} - \hat{\mathbf{n}} \cdot \mathbf{r}(t_{e,c})]$, so $\omega[c\Delta t_{e,c} - \hat{\mathbf{n}} \cdot \Delta \mathbf{r}(t_{e,c})]$ are the relative phases associated with a set of waves that reach optimal beaming at different times and places, and these waves add coherently for relative phases with magnitudes $\lesssim 1$. Note that the volumes constrained by Eq. (B2) represent *upper bounds*: actual volumes that emit coherently will depend on the emission mechanism. For example, for

charges that are all launched at the same place but at different times and travel along identical trajectories, hence reach optimal beaming at the same place, Eq. (B2) implies that the range of optimal beaming times is $\Delta t_{e,c} \lesssim r_c(2\kappa_{coh})^{3/2}$.

As an example, we consider motion along magnetic dipole field lines, $r = R_l \sin^2 \theta$. For a dipole field with symmetry axis along \hat{z} the unit vector tangent to a field line is

$$\hat{\mathbf{t}} = \frac{3 \cos \theta \hat{\mathbf{r}} - \hat{\mathbf{z}}}{\sqrt{3 \cos^2 \theta + 1}} = \frac{3 \cos \theta \sin \theta (\hat{\mathbf{x}} \cos \phi + \hat{\mathbf{y}} \sin \phi) + (3 \cos^2 \theta - 1) \hat{\mathbf{z}}}{\sqrt{3 \cos^2 \theta + 1}} \quad (\text{B3})$$

for angles θ, ϕ referenced to the dipole axis and the unit vector in the curvature direction is

$$\hat{\mathbf{c}} = \hat{\phi} \times \hat{\mathbf{t}} = \frac{(3 \cos^2 \theta - 1)(\hat{\mathbf{x}} \cos \phi + \hat{\mathbf{y}} \sin \phi) - 3 \cos \theta \sin \theta \hat{\mathbf{z}}}{\sqrt{3 \cos^2 \theta + 1}}. \quad (\text{B4})$$

Using $d\hat{\mathbf{t}}/ds = \hat{\mathbf{c}}/r_c$, the radius of curvature of a field line is

$$r_c = \frac{r(3 \cos^2 \theta + 1)^{3/2}}{3 \sin \theta (\cos^2 \theta + 1)}. \quad (\text{B5})$$

The direction to the observer is $\hat{\mathbf{n}} = \hat{\mathbf{x}} \sin \alpha + \hat{\mathbf{z}} \cos \alpha$. At the time of optimal beaming from a particular field line $\hat{\mathbf{n}} \cdot \mathbf{a} = 0 = \hat{\mathbf{n}} \cdot \hat{\mathbf{c}}$, since the acceleration \mathbf{a} is along $\hat{\mathbf{c}}$. At optimal beaming for a particular field line, $\hat{\mathbf{t}} \cdot \hat{\mathbf{n}} = \cos \epsilon \simeq 1 - \frac{1}{2} \epsilon^2 + \dots$; we define a reference field line to be the one for which $\epsilon = 0$, and $\theta = \theta(0)$ and $\phi = 0$. For any other point, optimal beaming occurs when $0 = -3 \cos \theta \sin \theta \cos \alpha + (3 \cos^2 \theta - 1) \sin \alpha \cos \phi$; we then find a displacement $\Delta \mathbf{r}$ whose components are

$$\begin{aligned} \hat{\mathbf{n}} \cdot \Delta \mathbf{r} &= \sin \theta(0) \left[\frac{2\Delta R_l \sin \alpha}{3} - \frac{\epsilon^2 R_l \cos \alpha (\sqrt{8 + \cos^2 \alpha} + \cos \alpha)^2}{8 \sin \alpha \sqrt{8 + \cos^2 \alpha}} \right] \\ \hat{\mathbf{c}}(0) \cdot \Delta \mathbf{r} &= -\frac{\Delta R_l (\sqrt{8 + \cos^2 \alpha} - 3 \cos \alpha)}{6} \\ \hat{\phi} \cdot \Delta \mathbf{r} &= \pm \frac{\epsilon R_l \sin^3 \theta(0)}{\sin \alpha}, \end{aligned} \quad (\text{B6})$$

where the contributions $\propto R_l$ come from either remaining on a field line but sliding along it or rotating azimuthally to another field line with the same R_l , and the contribution $\propto \Delta R_l$ comes from moving to a different (set of) field line(s). The coherence condition Eq. (B2) only involves the first component of Eq. (B6), but this condition constrains the other components indirectly.

First consider what happens when $\Delta t_{e,c} = 0$ i.e. find the volume when the coherent emission is simultaneous at the source. In that case, we can use Eq. (B2) to find $\Delta R_l/R_l$; unless $\epsilon \ll \gamma^{-3/2} \ll \gamma^{-1}$ we get $\Delta R_l/R_l = \epsilon^2 f_{\hat{\mathbf{n}}}(\cos \alpha)$, and therefore $\hat{\mathbf{c}}(0) \cdot \Delta \mathbf{r} = \epsilon^2 r_c f_{\hat{\mathbf{c}}}(\cos \alpha)$, where the functions are found by combining Eq. (B6) and (B2); $\hat{\phi} \cdot \Delta \mathbf{r} = \pm \epsilon r_c f_{\hat{\phi}}(\cos \alpha)$ is already determined by Eq. (B6). We therefore get an emitting area $\mathcal{A}_c = |\epsilon^3| r_c^2 f_{\mathcal{A}_c}(\cos \alpha) = (c r_c / \omega_{coh}) f_{\mathcal{A}_c}(\cos \alpha)$, and an emitting volume $\mathcal{V}_c = 2c / \omega_{coh} \times \mathcal{A}_c$ for an individual coherent pulse; explicitly

$$\mathcal{V}_c \lesssim \frac{64 c^2 r_c \sin \alpha \cos \alpha \sqrt{8 + \cos^2 \alpha}}{3 \omega_{coh}^2 (\sqrt{8 + \cos^2 \alpha} + \cos \alpha) (\sqrt{8 + \cos^2 \alpha} + 3 \cos \alpha)^2} \quad (\text{B7})$$

where Eq. (B2) implies $|\epsilon| \lesssim (c / \omega_{coh} r_c)^{1/3}$ and $|\hat{\mathbf{n}} \cdot \Delta \mathbf{r}| \lesssim c / \omega_{coh}$. Numerically, the characteristic upper limit on the volume for a set of charges emitting coherently with simultaneous $t_{e,c}$ are

$$\frac{c^2 r_c}{\omega_{coh}^2} = \frac{1.09 \times 10^{11} \text{ cm}^3 (r_c / r_{lc}) P}{\nu_{coh, \text{GHz}}^2}, \quad (\text{B8})$$

where the curvature radius has been expressed in units of $r_{lc} = cP/2\pi$, the light cylinder radius for spin

period P . Note that $\mathcal{V}_c \sim (\omega_{coh} r_c / c)(c / \omega_{coh})^3 \sim \epsilon^{-3}(c / \omega_{coh})^3 \sim \gamma^3(c / \omega_{coh})^3 \gg (c / \omega_{coh})^3$. The thickness of the volume along $\hat{\mathbf{n}}$ is $2c / \omega_{coh}$, so the coherent volume is severely flattened, with a cross-sectional area $\mathcal{A}_c \sim cr_c / \omega_{coh}$. The area is irregular, with a length $\sim r_c / \gamma^2 \sim \gamma c / \omega_{coh}$ along $\hat{\mathbf{c}}$ and $\sim r_c / \gamma \sim \gamma^2 c / \omega_{coh}$ along $\hat{\mathbf{n}} \times \hat{\mathbf{c}}$.

Note that this irregular shape arises from considering the largest possible region that can emit coherently, allowing the shape to be determined by Eq. (B2) and the magnetic field geometry. If the shape of the region emitting coherently is *prescribed* then it must fit entirely inside the largest possible coherently emitting region. For example, if we insist that coherent emission arises from a spherical region, then the radius of the sphere must be $\leq c / \omega_{coh}$, and the volume of the coherently emitting sphere is $\lesssim (c / \omega_{coh})^3$, as is often assumed. However, if the shape is not constrained to be regular, Eq. (B8) permits significantly larger coherently-emitting volumes.

The $\Delta t_{e,c} = 0$ limit is valid for $\Delta t_{e,c} \ll \epsilon^2 r_c / c$. For $\Delta t_{e,c} \gtrsim \epsilon^2 r_c / c \sim (\omega_{coh} \epsilon)^{-1} \sim \gamma / \omega_{coh}$, the time differences for optimal beaming are sufficiently non-simultaneous to affect the coherence volume substantially: the coherence condition is satisfied when $c \Delta t_{e,c} \simeq \hat{\mathbf{n}} \cdot \Delta \mathbf{r}$, or

$$\Delta R_l \simeq \frac{3c \Delta t_{e,c}}{2 \sin \theta(0) \sin \alpha}. \quad (\text{B9})$$

Eq. (B9) means that if the burst lasts a time $\Delta t_{e,c} \gtrsim \epsilon^2 r_c / c$ the point where emission is beamed right at the observer shifts through a succession of values of ΔR_l . We then find

$$\begin{aligned} \Delta \mathbf{r} \cdot \hat{\mathbf{c}}(0) &\simeq \frac{2c \Delta t_{e,c} \sin \alpha}{\sqrt{8 + \cos^2 \alpha} + 3 \cos \alpha} \\ \Delta \mathbf{r} \cdot \hat{\boldsymbol{\phi}} &\simeq \pm \frac{\epsilon R_l \sin^3 \theta(0)}{\sin \alpha}; \end{aligned} \quad (\text{B10})$$

the volume of the coherently emitting particles is

$$\mathcal{V}_c \lesssim \frac{4(c / \omega_{coh} r_c)^{1/3} r_c (c \Delta t_{e,c})^2 \sqrt{8 + \cos^2 \alpha} (\sqrt{8 + \cos^2 \alpha} - 3 \cos \alpha)}{3(\sqrt{8 + \cos^2 \alpha} + \cos \alpha)(\sqrt{8 + \cos^2 \alpha} + 3 \cos \alpha)}. \quad (\text{B11})$$

Eq. (B11) differs from Eq. (B7) by a factor $\sim (\omega_{coh} \Delta t_{e,c})^2 \gamma^{-1} \gtrsim \gamma$. The shape of the coherent region is irregular, but $|\hat{\mathbf{n}} \cdot \Delta \mathbf{r}| \sim |\hat{\mathbf{c}}(0) \cdot \Delta \mathbf{r}| \sim c \Delta t_{e,c}$ in this case, while $|\hat{\boldsymbol{\phi}} \cdot \Delta \mathbf{r}| \sim r_c / \gamma$. If $\Delta t_{e,c} \sim r_c / c \gamma = P(r_c / r_{lc}) / 2\pi \gamma = 0.16 P(r_c / r_{lc}) \gamma_3^{-1}$ ms then the extent of the region is similar in all three directions.

We have focussed on dipole field geometry in this section, but we expect many of the scalings to remain valid if $r = R_l \mathcal{F}(\sin \theta)$, where $\mathcal{F} = \sin^2 \theta$ for a dipolar field; that is, although the dependences on α will differ, if the field line shapes only depend on a single length scale, then similar results should be obtained. Realistically, though, the shapes of pulsar magnetic field lines will depend on at least two lengths, R_l and the light cylinder radius r_c , and the situation is more complicated. However, to the extent that only localized regions are involved in coherent emission, and assuming that field lines may be approximated as circular locally, the basic results we found for the extent of coherent regions ought to be similar to what we found here for dipole geometry.

REFERENCES

- Arnaud, M., Pratt, G. W., Piffaretti, R., et al. 2010, *AAp*, 517, A92
- Arons, J., & Scharlemann, E. T. 1979, *ApJ*, 231, 854
- Arzoumanian, Z., Chernoff, D. F., & Cordes, J. M. 2002, *ApJ*, 568, 289
- Asseo, E., & Porzio, A. 2006, *MNRAS*, 369, 1469
- Bahcall, N. A. 1996, arXiv:astro-ph/9611148
- Bahcall, N. A. 1999, *Formation of Structure in the Universe*, 135
- Bannister, K. W., & Madsen, G. J. 2014, *MNRAS*, 440, 353
- Barnard, J. J., & Arons, J. 1986, *ApJ*, 302, 138
- Bauer, A. H., Baltay, C., Ellman, N., et al. 2012, *ApJ*, 749, 56
- Benford, G., & Buschauer, R. 1977, *MNRAS*, 179, 189
- Burke-Spolaor, S., Bailes, M., Ekers, R., Macquart, J.-P., & Crawford, F., III 2011, *ApJ*, 727, 18
- Burke-Spolaor, S., Johnston, S., Bailes, M., et al. 2012, *MNRAS*, 423, 1351
- Burke-Spolaor, S., & Bannister, K. W. 2014, *ApJ*, 792, 19
- Buschauer, R., & Benford, G. 1976, *MNRAS*, 177, 109
- Buschauer, R., & Benford, G. 1978, *MNRAS*, 185, 493
- Buschauer, R., & Benford, G. 1980, *MNRAS*, 190, 945
- Cheng, A. F., & Ruderman, M. A. 1979, *ApJ*, 229, 348
- Connor, L., Sievers, J., & Pen, U.-L. 2015, arXiv:1505.05535
- Cordes, J. M. 1976, *ApJ*, 210, 780
- Cordes, J. M., & Lazio, T. J. W. 2002, arXiv:astro-ph/0207156
- Cordes, J. M., & McLaughlin, M. A. 2003, *ApJ*, 596, 1142
- Cordes, J. M., Bhat, N. D. R., Hankins, T. H., McLaughlin, M. A., & Kern, J. 2004, *ApJ*, 612, 375
- Cordes, J. M., & Shannon, R. M. 2008, *ApJ*, 682, 1152
- Crawford, F., Altemose, D., Li, H., & Lorimer, D. R. 2013, *ApJ*, 762, 97
- Crossley, J. H., Eilek, J. A., Hankins, T. H., & Kern, J. S. 2010, *ApJ*, 722, 1908
- Dennison, B. 2014, *MNRAS*, 443, L11
- Dolag, K., Gaensler, B. M., Beck, A. M., & Beck, M. C. 2015, *MNRAS*, 451, 4277
- Falcke, H., & Rezzolla, L. 2014, *AAp*, 562, AA137
- Goldreich, P., & Julian, W. H. 1969, *ApJ*, 157, 869
- Goldreich, P., & Keeley, D. A. 1971, *ApJ*, 170, 463
- Gwinn, C. R., Johnson, M. D., Smirnova, T. V., & Stinebring, D. R. 2011, *ApJ*, 733, 52
- Hankins, T. H., & Rickett, B. J. 1975, *Methods in Computational Physics*, 14, 55
- Hankins, T. H., Kern, J. S., Weatherall, J. C., & Eilek, J. A. 2003, *Nature*, 422, 141
- Hankins, T. H., & Eilek, J. A. 2007, *ApJ*, 670, 693
- Hogg, D. W. 1999, arXiv:astro-ph/9905116
- Jackson, J. D. 1962, *Classical Electrodynamics*, New York: Wiley.
- Jauch, J. M., & Rohrlich, F. 1976, *The Theory of Photons and Electrons*, New York: Springer, 2nd ed.
- Johnston, S., & Romani, R. W. 2003, *ApJL*, 590, L95
- Katz, J. I. 2014, *Phys. Rev. D*, 89, 103009
- Katz, J. I. 2014, arXiv:1409.5766
- Katz, J. I. 2015, arXiv:1505.06220
- Keane, E. F., Kramer, M., Lyne, A. G., Stappers, B. W., & McLaughlin, M. A. 2011, *MNRAS*, 415, 3065
- Keane, E. F., & Petroff, E. 2015, *MNRAS*, 447, 2852
- Kinkhabwala, A., & Thorsett, S. E. 2000, *ApJ*, 535, 365
- Kramer, M., Lyne, A. G., O'Brien, J. T., Jordan, C. A., & Lorimer, D. R. 2006, *Science*, 312, 549
- Kronberg, P. P., Bernet, M. L., Miniati, F., et al. 2008, *ApJ*, 676, 70
- Kulkarni, S. R., Ofek, E. O., Neill, J. D., Zheng, Z., & Juric, M. 2014, *ApJ*, 797, 70
- Law, C. J., Bower, G. C., Burke-Spolaor, S., et al. 2015, *ApJ*, 807, 16
- Loeb, A., Shvartzvald, Y., & Maoz, D. 2014, *MNRAS*, L2
- Lorimer, D. R., Bailes, M., McLaughlin, M. A., Narkevic, D. J., & Crawford, F. 2007, *Science*, 318, 777
- Lorimer, D. R., Karastergiou, A., McLaughlin, M. A., & Johnston, S. 2013, *MNRAS*, 436, L5

Luan, J., & Goldreich, P. 2014, *ApJL*, 785, LL26
 Lundgren, S. C., Cordes, J. M., Ulmer, M., et al. 1995, *ApJ*, 453, 433
 Madau, P., & Dickinson, M. 2014, *ARAA*, 52, 415
 McQuinn, M. 2014, *ApJL*, 780, L33
 McLaughlin, M. A., Lyne, A. G., Lorimer, D. R., et al. 2006, *Nature*, 439, 817
 Michel, F. C. 1982, *Reviews of Modern Physics*, 54, 1
 Michel, F. C. 1991, *Theory of Neutron Star Magnetospheres*, Chicago: University of Chicago Press
 Mickaliger, M. B., McLaughlin, M. A., Lorimer, D. R., et al. 2012, *ApJ*, 760, 64
 Nagai, D., Kravtsov, A. V., & Vikhlinin, A. 2007, *ApJ*, 668, 1
 Olausen, S. A., & Kaspi, V. M. 2014, *ApJSuppl*, 212, 6
 Oppermann, N., Junklewitz, H., Robbers, G., et al. 2012, *AAp*, 542, A93
 Osłowski, S., van Straten, W., Hobbs, G. B., Bailes, M., & Demorest, P. 2011, *MNRAS*, 418, 1258
 Papoulis, A. 1991, "Probability, Random Variables, and Stochastic Processes," (McGraw-Hill, New York), pp. 629-635
 Petroff, E., Bailes, M., Barr, E. D., et al. 2015, *MNRAS*, 447, 246
 Petroff, E., Johnston, S., Keane, E. F., et al. 2015, *MNRAS*, 454, 457
 Petroff, E., Keane, E. F., Barr, E. D., et al. 2015, arXiv:1504.02165
 Planck Collaboration, Ade, P. A. R., Aghanim, N., et al. 2014, *AAp*, 571, A29
 Planck Collaboration, Ade, P. A. R., Aghanim, N., et al. 2015, arXiv:1502.01597
 Planck Collaboration, Ade, P. A. R., Aghanim, N., et al. 2015, arXiv:1502.01598
 Ravi, V., Shannon, R. M., & Jameson, A. 2015, *ApJL*, 799, L5
 Reiprich, T. H. & Böhringer, H. 2002, *ApJ*, 567, 716
 Read, J. I., & Trentham, N. 2005, *Royal Society of London Philosophical Transactions Series A*, 363, 2693
 Rees, M. J. 1977, *Nature*, 266, 333
 Rice, S. O. 1944, *Mathematical Analysis of Random Noise*, Bell System Technical Journal, 23: 3, pp 282-332. Reprinted in Wax, N. *Noise and Stochastic Processes*, (Dover, New York), pp. 133-183.
 Rickett, B. J. 1975, *ApJ*, 197, 185
 Rines, K., Diaferio, A., & Natarajan, P. 2007, *ApJ*, 657, 183
 Rozo, E., Rykoff, E. S., Evrard, A., et al. 2009, *ApJ*, 699, 768
 Rozo, E., Bartlett, J. G., Evrard, A. E., & Rykoff, E. S. 2014, *MNRAS*, 438, 78
 Ruderman, M. A., & Sutherland, P. G. 1975, *ApJ*, 196, 51
 Sallmen, S., Backer, D. C., Hankins, T. H., Moffett, D., & Lundgren, S. 1999, *ApJ*, 517, 460
 Saint-Hilaire, P., Benz, A. O., & Monstein, C. 2014, *ApJ*, 795, 19
 Schmekel, B. S. 2005, *Phys. Rev. E*, 72, 026410
 Schmekel, B. S., & Lovelace, R. V. E. 2006, *Physical Review Special Topics Accelerators and Beams*, 9, 114401
 Schmekel, B. S., Lovelace, R. V. E., & Wasserman, I. M. 2005, *Phys. Rev. E*, 71, 046502
 Spitler, L. G., Cordes, J. M., Hessels, J. W. T., et al. 2014, *ApJ*, 790, 101
 Sturrock, P. A. 1970, *Nature*, 227, 465
 Sturrock, P. A. 1971, *ApJ*, 164, 529
 Tempel, E., Tamm, A., Gramann, M., et al. 2014, *AAp*, 566, A1
 Thornton, D., Stappers, B., Bailes, M., et al. 2013, *Science*, 341, 53
 Tully, R. B., Courtois, H., Hoffman, Y., & Pomarède, D. 2014, *Nature*, 513, 71
 Voit, G. M. 2005, *Reviews of Modern Physics*, 77, 207
 Weatherall, J. C. 1998, *ApJ*, 506, 341
 Weatherall, J. C. 2001, *ApJ*, 559, 196
 Weatherall, J. C., & Benford, G. 1991, *ApJ*, 378, 543
 Wen, Z. L., Han, J. L., & Liu, F. S. 2010, *MNRAS*, 407, 533
 Xu, Y., Kronberg, P. P., Habib, S., & Dufton, Q. W. 2006, *ApJ*, 637, 19
 Yu, Y.-W., Cheng, K.-S., Shiu, G., & Tye, H. 2014, *Journal of Cosmology and Astroparticle Physics*, 11, 040

Zheng, Z., Ofek, E. O., Kulkarni, S. R., Neill, J. D., & Juric, M. 2014, *ApJ*, 797, 71